

TECHNOLOGY MIGRATION FOR HARD IPS

by

Fang Fang

A thesis submitted in conformity with the requirements
for the degree of Master of Applied Science
Graduate Department of Electrical and Computer Engineering
University of Toronto

Copyright © 2003 by Fang Fang

Abstract

Technology Migration for Hard IPs

Fang Fang

Master of Applied Science

Graduate Department of Electrical and Computer Engineering

University of Toronto

2003

As the foundries accelerate their update of advanced processes with increasingly complex design rules, the cost of hard intellectual property (IP) development becomes prohibitively high. A technology migration tool that can port hard IPs from old technology to new technology is presented in the thesis. The thesis makes four primary contributions: First, it proposes a new fast design rule constraint generation algorithm that further limits the searching spaces. Second, it introduces a dual-pass strategy to solve the high level layout architecture constraints for migrating all the library leaf cells. Third, it proposes a new optimization metric, called geometric closeness, that can help retain advanced design intention. Finally, soft constraints method is proposed to trace the conflicting constraints specified by the users. We test our migration tool by successfully migrating Berkeley low power libraries, originally developed for 1.2um MOSIS process to TSMC 0.25um and 0.18um technologies.

Acknowledgements

Contents

1	Introduction	1
1.1	Motivation	3
1.2	Contribution	3
1.3	Organization of thesis	4
2	Background	5
2.1	Virtual Grid Compaction and Shear-line Compaction	5
2.2	Constraint Graph Compaction	7
2.3	Hierarchical Layout Compaction	11
2.4	Other Developments	12
3	Migration Engine	15
3.1	Background	15
3.2	Migration Engine	28
3.3	Design Rule Constraint Generation	30
3.4	Objective function	46
3.5	Integer Linear Programming Solver	51
4	Migration for datapath and standard cell libraries	52
4.1	Datapath library migration	52
4.2	Standard Cell Library Migration	61

5	Experiments and Conclusion	67
5.1	Experimental Setup	67
5.2	Experimental Result	68
5.3	Limiation	76
5.4	Conclusion	78
5.5	Future work	79
6	Appendix	80
	Bibliography	96

List of Tables

5.1	Layout architecture characteristics	71
5.2	Layout structure characteristics	75
5.3	User specified layout architecture requirements for cell haf001	78
6.1	Experiment results of datapath library migration.	82
6.2	Experiment results for standard cell library migration.	84

List of Figures

1.1	A general architecture of SoC.	2
2.1	Before virtual grid compaction.	6
2.2	After virtual grid compaction.	6
2.3	A spacing constraint is presented by an edge in the directed graph.	7
2.4	A's shadow is blocked by B. So there is no edge between A ad C in the constraint graph.	8
2.5	Each circuit element is expanded by $D/2$ in both positive and negative X directions. The elements that stay within the same slot in scanning bar are recorded in the same X coordinate bin.	9
2.6	The constraint graph for a cell to be pitch matched.	11
2.7	Port abstraction method.	12
2.8	Wire jogging.	13
3.1	A layout is composed of several planes.	16
3.2	The tile structure in metal1 plane	18
3.3	The process to find right neighbor tiles.	21
3.4	The process to locate the tile that contains a given point	23
3.5	Tile enumeration.	26
3.6	Each edge rule can be applied in any of the four directions.	26
3.7	An example of edge rule.	27

3.8	Tiles are aligned in grids	29
3.9	Each tile has new position and shape after migration with no design rule violations.	30
3.10	Design rule checker looks for non-OKType tiles within constraint region. . . .	31
3.11	(a) An example layout in active plane. The shaded rectangles 1, 3, 5, 6 and 10 represent poly tiles. Rectangle 8 is diffusion tile. Other rectangles are all space tiles. (b) The constraint graph generated from poly spacing rule.	32
3.12	(a) A fraction of a layout plane. Tile 1 is the source tile that is being processed for edge rule constraint generation. (b) Depth-K shadowing neighborhood graph for tile 1.	34
3.13	The best case for Depth-K searching algorithm	37
3.14	The maximum number of tiles to be visited for tile s	38
3.15	A leaf cell muxf201.	38
3.16	The constraint graph for IntraPlane constraints.	39
3.17	Corner constraint region checking	39
3.18	(a) In the old layout, tile 3 doesn't overlap with tile s in X direction. (b) After X direction migration and Y direction migration, tile 3 moves into shadow area of tile 1. (c) Interpass Constraint graph for tile s (d) Interpass constraints for tile s.	40
3.19	N-well tile stays on well plane while diffusion tile stays on active plane. . . .	42
3.20	(a)The Depth-K shadowing neighborhood graph for interplane edge rule (b) InterPlane edge rule constraint between source tile s and tile 3.	43
3.21	InterPlane constraints generated for cell muxf201.	44
3.22	A contact has different tile types on the planes it connects. The poly contact in this figure has pcontact tile (tile 1) on active plane and pcontact/metal1 tile (tile 2) on metal1 plane.	45
3.23	Connect constraints generated for cell muxf201.	46

3.24	Tile 1 is the leftmost tile in a layout and x_l is the X coordinate of its left edge. Tile 2 is the rightmost tile in the layout and x_r is the X coordinate of its right edge.	47
3.25	The old layout and migrated layout with minimum perturbation objective func- tion.	49
3.26	The old layout and migrated layout with geometric closeness objective function.	50
4.1	An 8-bit adder block diagram.	53
4.2	An 8-bit adder constructed by abutting 8 adder bitslices and 1 control slice. . .	54
4.3	An example of datapath library cell.	54
4.4	Port matching of leaf cells.	55
4.5	Dual-pass migration strategy.	57
4.6	Cell with routing track for data signals.	58
4.7	The width of each power net has to be equal to pw given by the designer in the specification file.	59
4.8	Standard cells design	62
4.9	Layout architecture for a standard cell library.	63
4.10	All I/O ports stay in fixed grids	64
4.11	The requirements on power rails	65
5.1	The run time of design rule constraint generation	69
5.2	The run time of ILP solver.	70
5.3	The leafcells for ripple carry adder	71
5.4	The floorplane of an N bit adder.	72
5.5	Migration of a four-bit adder	73
5.6	Two old standard cells based on standard MOSIS $1.2\mu m$ technology.	74
5.7	Migrated cells based on TSMC $0.18\mu m$ technology.	74

5.8	The migration results under geometric closeness objective function and minimum perturbation objective function.	76
5.9	Cell haf001 before migration	76
5.10	Cell haf001 after migrated towards TSMC 0.18 μm technology.	77
5.11	The design rule requirements on power rail.	77

Chapter 1

Introduction

The ASIC technology has evolved from a chip-set philosophy to system-on-chip (SoC) concept. SoC is generally defined as *an IC designed by stitching multiple stand-alone VLSI designs to provide full functionality for an application* [21]. A general architecture of today's SoC is shown in Figure 1.1. The definition of SoC implies that the complexity of SoC is greatly increased compared to ASIC. And with the time-to-market pressure, the SoC designers are tuning to block-based design approach that emphasis on design reuse in order to achieve fast development. The macros, also called intellectual-properties (IPs), usually come in two forms: *soft IPs*, delivered in the form of synthesizable RTL code, and *hard IPs*, delivered in the form of fully placed and routed netlist and fixed layout mapped to a specific technology. There are some trade-offs between choosing hard IPs and choosing soft IPs for block reuse. Since the soft IPs can be re-synthesised by the SoC integrators for their chosen technology, they are favored in terms of their portability and re-usability. On the other hand, the hard IPs have a physical representation, and are delivered in the form of layout file such as GDSII file. The SoC is essentially a combination of these hard IPs that implement function blocks such as memories, microprocessors in Figure 1.1. Therefore, they are more predictable than soft IPs in terms of timing, power and area and result in less effort during SoC integration.

The primary bottleneck that prevents wide adoption of hard IPs is the dependency of layout

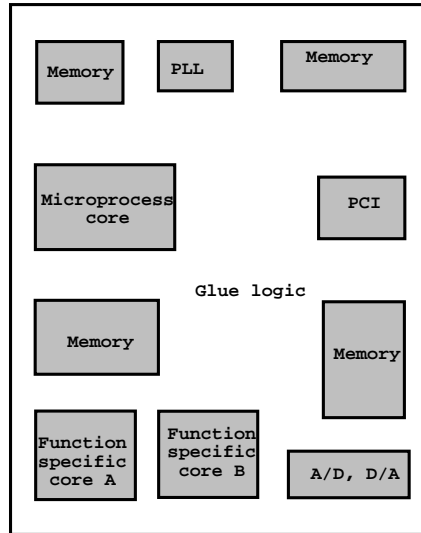


Figure 1.1: A general architecture of SoC.

on process. In standard ASIC design, a library with a rich selection of gates with different drive strengths, buffer sizes and dual polarities for functions must be provided to IC designers. Today's standard cell library contains hundreds of leaf cells with different functions and different drive lengths. There are many unique design considerations such as porosity, aspect ratio, power distribution, etc., related to physical design of these libraries. It takes great design effort to create such libraries from scratch. Therefore most fabless companies choose to use libraries offered by hard IP companies to avoid the high cost associated with library development. To make things worse, manufacturing processes are updated every 18 months, each time using a different set of design rules. This makes the development cost of hard IPs too high even for hard IP vendors, since they have to offer different versions for different foundries as well. Automatic layout migration technology, which can port libraries from old technology to new technology and thus amortize the high development cost associated with custom design across different foundries and processes, is therefore crucial for the sustained growth of IP-based design.

1.1 Motivation

Layout migration tools available today cannot cope with all the challenges involved. First, most migration tools are based on layout compaction, a technology developed a decade ago, when the layout area is the primary concern. Layout compaction tends to compress space between polygons recklessly as long as design rules are not violated. In modern design using aggressive circuit styles in deep submicron processes, space is often among the first class citizens of *advanced layout considerations*, for example, to combat signal integrity. Other specialized *advanced circuit considerations*, such as new transistor sizes, device matching, are rarely considered in an integrated fashion. Second, most techniques reported in the literature are designed to migrate a specific circuit that uses a library of cells, rather than the library itself. Without considering the *overall library architecture* such as power/ground net width, routing track number and port matching, the cell layouts migrated under this circuit-driven strategy work only for the specific circuits, so there is no guarantee that they work under all occasions, and each time a new circuit is migrated, all the leaf cells in the whole library need to be migrated again.

1.2 Contribution

An integer linear programming (ILP) based migration framework which is customized for datapath IP and standard cell IP migration is presented in this thesis. New libraries based on new technologies can be generated when given the libraries of the old process and new library architecture specifications. Several innovations that help solve the difficult problems discussed earlier are listed below:

- A new design rule generation algorithm, *Depth-K searching algorithm*, which takes less searching effort than the shadow propagation method currently employed for constraint generation [18], is used in this project.

- A new optimization objective, called *geometric closeness*, to reward geometric resemblance of migrated layout to the original layout is introduced in this project. Under this metric, space is explicitly represented. Preservation of space and non-space polygons is given equal priority. This ensures that the original layout design considerations are not corrupted
- In order to address the overall library architecture requirements, a *dual-pass strategy* is employed in the migration tool that helps meet high level layout architecture constraints. This is in contrast to the top-down constraint propagation strategy employed by traditional hierarchical compactors, which are limited only to area minimization.
- Since the library architecture is specified by users, they may conflict with design rules, which will lead to an infeasible solution. A new concept, called *soft constraints*, is proposed in order to obtain a best-effort solution. A concrete feedback is provided where architecture requirements fail, which thereby helps the user interactively define the proper library architecture.

1.3 Organization of thesis

The rest of the thesis is organized as follows: First a review of previous work is given in chapter 2. Then a detailed discussion of the basic migration engine implementation is presented in chapter 3. Chapter 4 talks about what are the specific layout architecture requirements for datapath library and standard cell library and how the requirements are solved with the dual-path approach. The experimental results are given in Chapter 5. Finally, Chapter 6 gives the conclusion and summarizes the future work.

Chapter 2

Background

Automatic layout migration was among the oldest CAD problems investigated and a large body of research was carried out under the layout compaction problem. Surveys of layout compaction can be found in [6] and [9]. Early compactors are performed on symbolic layout in which circuit elements are presented by simple lines or rectangles, known as *sticks*. The symbolic layout compaction methodologies include shear-line approach, virtual grid approach and constraint graph approach, which will be discussed in the following sections.

2.1 Virtual Grid Compaction and Shear-line Compaction

Commercial layout systems such as **MULGA** [25] use the virtual grid compaction approach to compress the layout. Once the symbolic layout is generated, the virtual grid compaction method compresses space by moving objects. The procedure includes two main steps:

- search for movable objects by consultation with layout topology and design rules;
- perform the compaction by moving these objects.

In order to identify the movable objects and the moving distance, the layout is represented by a $m \times n$ matrix as shown in Figure 2.1. Each entry of the matrix represents a mask element marked as a shaded cell or space marked as a blank cell. The size of the grid unit is determined

by design rules. Objects are restricted to one unit move usually. The movable objects are decided by searching for a path of blank cells across the matrix. The path could be a straight line or a union of straight lines connected as shown in Figure 2.1. Therefore, the compaction is proceeded by repeatedly removing paths along X and Y direction until no path could be found. The migrated layout is shown in Figure 2.2.

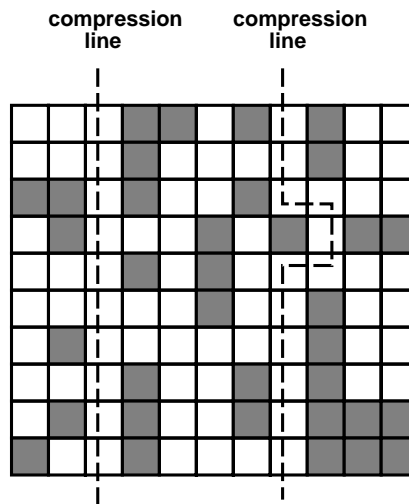


Figure 2.1: Before virtual grid compaction.

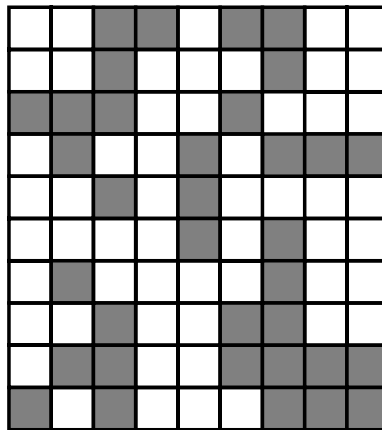


Figure 2.2: After virtual grid compaction.

The shear-line approach is very similar to virtual grid compaction except that the grid spacing is fixed to the worst case design rule [8] [1].

The compaction is made easy with the matrix representation of the layout. However, the grid size must be carefully decided because coarse grid results in smaller matrix and thus less run time, but the compaction may not be efficient. On the other hand, high grid resolution will lead to large matrix and thus slow down the run time. Another disadvantage of this compaction method is that the optimization goal can only be the minimization of the layout area. With this approach, no other optimization goals can be achieved.

2.2 Constraint Graph Compaction

The constraint graph compaction was first discussed by Hsueh and Pederson [18]. Many other compaction tools such as **FLOSS** [5], **CABBAGE** [18] and **SLIM** [1], use this strategy to compact layouts. In this approach, the topology constraints and design rule requirements are presented with a weighted directed graph, called *constraint graph*. Each vertex represents a circuit element. For each spacing constraint between two elements, there is an arc (i, j) with weight d_{ij} .

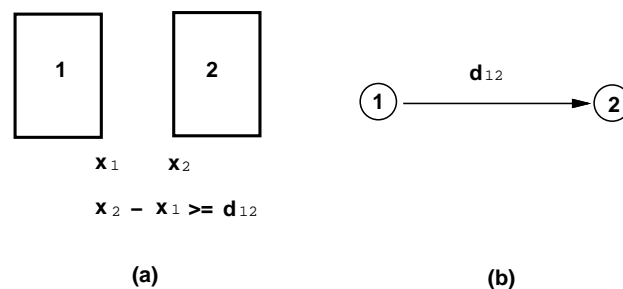


Figure 2.3: A spacing constraint is presented by an edge in the directed graph.

The new position of each element can be obtained either by running longest path algorithm or by using linear programming solver depending on the optimization goal the user chooses. Because of its flexibility, we adopt this approach in our migration tool.

2.2.1 Constraint Generation

The key part of constraint graph compaction is design rule constraint generation, which is used to identify the spacing relationship among all the elements according to design rules and layout topology. The constraint generation process is very similar to design rule checking except that the circuit elements outside of checking region need to be considered as well because they may be pushed into the checking region after compaction. One of the most often used methods to generate constraints is called “shadow-propagation” method used in CABBAGE [18]. This approach trims the searching area by shining an imaginary light from the element being checked as shown in Figure 2.4. Based on the assumption that the relative positions between two elements will not be changed, which means that the element C will not move to the shadow of element A in Figure 2.4, only the constraints between the given element and the elements that the shadow first meet are generated. The worst case complexity for shadow-propagation method is proven to be $O(N^{1.5})$, where N is the total number of elements in the symbolic layout. With the experimental result, the experimental complexity is found to be $O(N^{1.2})$.

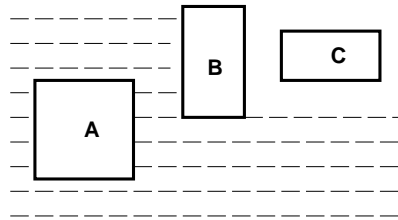


Figure 2.4: A’s shadow is blocked by B. So there is no edge between A and C in the constraint graph.

Another approach to generate constraints come from a design rule checking method called *scan line approach* [20], which is demonstrated in Figure 2.5. The circuit elements that stay too far from the checking element are filtered out by the scanning bar of width D , which is the worst-case design rule distance. The X coordinate bins record all the circuit elements for design rule checking. There are two key issues related with this approach. First, the number

of bins in the X direction must be carefully decided. Too few bins may cause the missing of constraints. On the other hand, too many bins results in redundant constraints as the same pair of elements may occupy many bins. The scan line approach sets the bin number according to statistical analysis of element density so that each pin covers 2.52 elements on average. The other key issue is that iterative sorting of the shape record buffer when adding or deleting elements. The experimental data indicate that with N elements in the layout, the expected time complexity required is $O(N \log(N))$ [20].

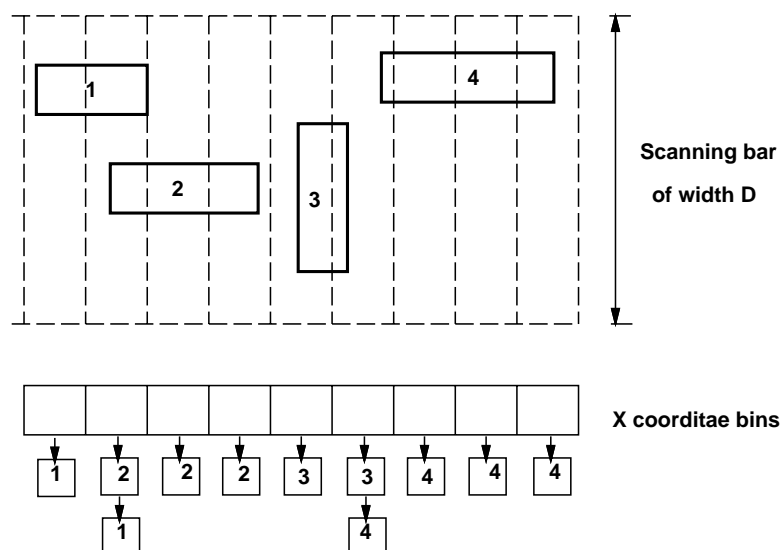


Figure 2.5: Each circuit element is expanded by $D/2$ in both positive and negative X directions. The elements that stay within the same slot in scanning bar are recorded in the same X coordinate bin.

With constraint graph generated, some techniques are used to reduce the redundant edges and thus reduce the complexity of solving the constraint graph. The intervening group method incrementally generates the the constraint graph by effectively avoiding adding vertices when a pair of vertices are constrained to be far enough [12]. A combination of shadowing-propagation and binning is proposed with worst case complexity claimed to be $O(N^{1.5})$. All these techniques are based on the shadowing-propagation method to build constraint graph and remove the unnecessary edges after the constraint graph is generated.

The constraint generation methods discussed above are all performed on symbolic layout. In symbolic layout, the circuit elements such as transistor, contact and wire are modelled as sticks snapped to virtual grids. At symbolic layout level, circuit elements do not have detailed mask information. The positions of circuit elements are decided by respecting the high level design rules such as minimum spacing rules and minimum width rule, etc. In order to generate real mask layout, another process to transform symbolic layout to mask layout is needed after symbolic layout compaction. In this thesis, we directly migrate the mask layout without taking the symbolic layout transformation step. A new constraint generation method applied directly on mask layout represented in corner stitching data structure, called *Depth-K searching algorithm*, is proposed in this thesis that can further reduce the searching area by limiting the depth it traverses than the shadowing-propagation algorithm. And with corner stitching layout representation, it avoids the iterative sorting of shape buffers in scan line approach. The data in the Appendix show that the experimental run time is proportional to $O(N^{1.4})$.

2.2.2 Objective Function

After the constraint graph is built, there are two ways to solve the graph. One is to decide each vertex's longest path length from the boundary vertex, which amounts to finding the shortest path algorithm in a directed graph with arc weight negated. Most of early compaction tools are based on this approach. However, the implied compaction goal of this approach is to minimize the layout area. In order to accommodate more compaction goals such as minimization of power or perturbation, the constraint graph is solved by dumping constraints to linear programming solver and obtaining the result under the user specified compaction goal.

The *minimum perturbation objective function* proposed in [10] was the first work that departed from the traditional area minimization optimization goal and argued the importance of rewarding geometric similarity between the migrated layout and the original layout. However, the quantitative measure that they develop for geometric similarity is asymmetrical and penalizes both right edges in the X direction and upper edges in the Y direction. In our migration

tool, we slightly modify the minimum perturbation objective function by minimizing the size change of each rectangle in the layout.

2.3 Hierarchical Layout Compaction

The majority of the hierarchical layout compactors reported in literature focus on solving the pitch matching problem, which means that certain elements among different cells must match in size and position when cells are abutted. The method described in [11] first compacts leaf-cells and then locates the abutting ports to fixed grids. After that, the compacted cells are assembled and compacted at the higher level of hierarchy as shown in Figure 2.6 [9]. In this method, routing is needed to guarantee the connection.

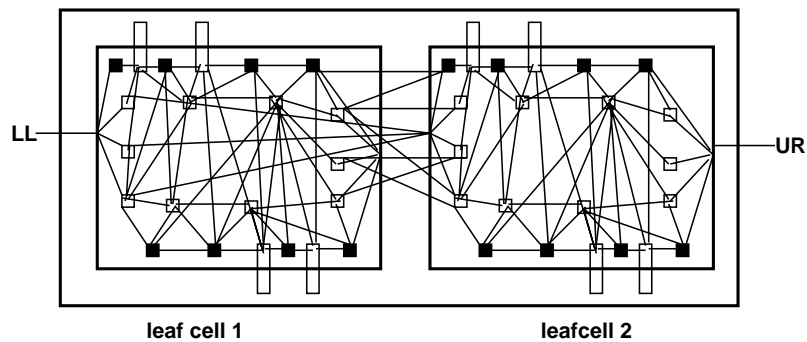


Figure 2.6: The constraint graph for a cell to be pitch matched.

The pitch matching method introduced in [15] matches the abutting ports by directly adding abutting constraints between cells to the constraint graph. This method assumes that hierarchical layout is given. The constraints for all leafcells have to be dumped to linear programming solver so that port matching constraints can be solved. As the number of leafcells increases, this method will be limited by the capability of linear programming solver.

A powerful pitch matching algorithm is reported in [13] based on port abstraction method. The port abstraction graph can be considered as a simplification of the constraint graph for each

cell, where constraints unrelated to the ports are removed as shown in Figure 2.7. The longest path between ports are computed and the port locations of each cell are then solved by solving the combined port abstraction graph of the circuit that uses the cell to be migrated. The result is then set as constraints to drive the migration of each leaf cell. The port abstraction method is very powerful in solving pitch matching problem. However, the main problem related is that the port position is decided by the longest path algorithm, which means that the ports will be placed as close as possible to each other. It implies that the total layout area will be minimized and it is not suitable to handle other objective functions. So our migration tool takes another approach called *Dual-pass strategy* that can decide port locations with considerations of both design rules and the objective function.

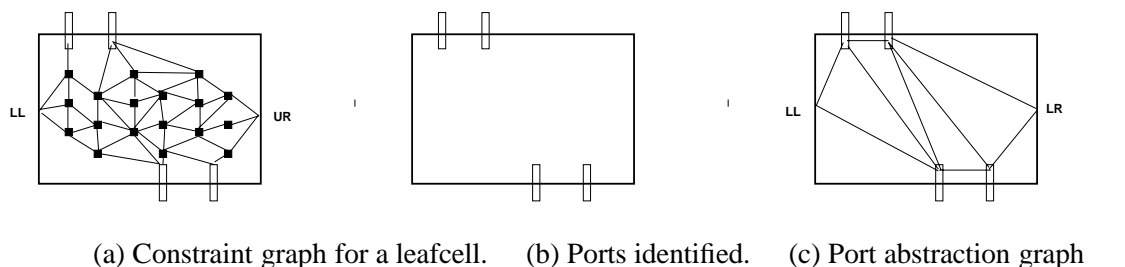


Figure 2.7: Port abstraction method.

2.4 Other Developments

The automatic jogging wires and wire length minimization are the two problems that have been investigated together with compaction problem. One of the first approach for wire jogging was presented in [18]. In this approach, the wire is bended at the “torque” points on a straight wire as shown in Figure 2.8.

The usage of wire jogging is limited because it could reduce the layout size in one direction but potentially, increasing the size in another direction [9]. In our project, we introduce the geometric closeness objective function to keep the original shape of the layout to a maximum extent. The wire jogging will introduce big changes to the layout, therefore, it is not considered

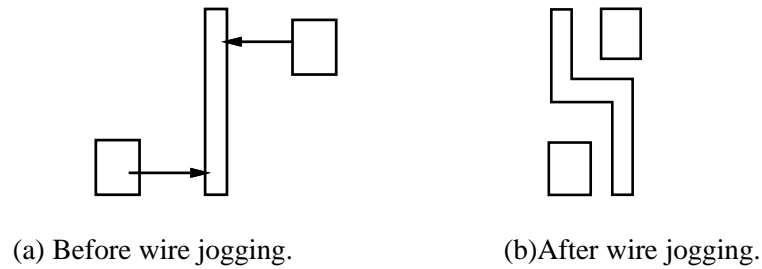


Figure 2.8: Wire jogging.

in our tool.

Another effort has been spent on minimizing the wire length on critical path. This is achieved by uniformly distributing spaces among circuit elements [18] or by “pulling” circuit elements back so that the length of connection wire is not increased drastically. As our migration tool could minimize the wire length by migrating layouts under minimum area objective function, we will not include this step in our tool.

As fabrication technology in the IC industry advances, some foundries are demanding the use of more complicated rules such as conditional design rules. For example, some conditional rules require that the spacing of two edges depend on the context in which edges are situated [4]. Finding the optimal solution under conditional rule has been proven to be NP-complete. However, some heuristic method has been reported that can solve compaction under simplified conditional rules: bridge rules [4]. This algorithm has some potential applications. On the other hand, solving the conditional rule depends on the correct design rule modelling. The edge rule system we use currently has accommodated conditional rules. So our tool does not take this issue into account.

All the compaction methods discussed above are one-dimensional compaction. Several techniques have been proposed for simultaneous two-dimensional compaction [17] [26]. The methodologies mainly include two steps. First, the compact layouts without respecting minimum distance requirements. Then select each pair of elements and add spacing constraints that could be in the X direction or in the Y direction. Compared to one-dimensional compaction, two-dimensional compaction methodology has not been widely used. The main reason is that

two-dimensional compaction is proven to be NP-complete [17] [6]. The effectiveness of these heuristic algorithms needs to be further verified. And with the X compaction and Y compaction performed together, the layouts have more freedom for topology changes. Therefore, we still adopt the traditional one-dimensional compaction approach for our migration tool.

Chapter 3

Migration Engine

3.1 Background

Layout and design rules are the objects that a migration tool processes. This section reviews the layout representation methodology and design rule modeling methodology. In the text that follows, we use the *formal algorithm notation* (FAN) to state definitions and describe algorithms [27]. FAN relies on a type system, where each type is presented by a set, to present the algorithm in a formal, precise manner. For example, we use the notation $\langle \rangle^A$ to represent the power set of A, therefore, any value of type $\langle \rangle^A$ will be a set of values of type A. Readers are expected to find this notation very similar to any strongly-typed programming languages and hence be translated into implementation.

3.1.1 Layout Representation

A layout is a drawing of a set of polygons, each associated with a different layer, such as metal, poly, or diffusion, given by the fabrication technology. For simplification, polygons are often constrained to be rectangular, called *Manhattan layout*, and polygons related by their layers are organized in logical layers, called *planes*, as shown in Figure 3.1.

3.1.2 Corner stitching

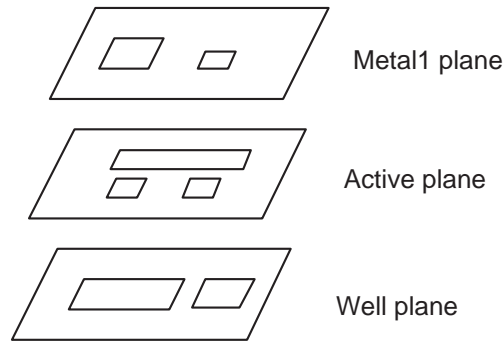


Figure 3.1: A layout is composed of several planes.

Choosing a good layout representation is a key to producing fast geometric operations for migration tools. In this project, a data structure called *corner stitching* which can provide fast operations such as neighbor finding is used to represent the layout [19]. A brief discussion of the corner stitching algorithm is given in this section.

We first define **Technology** and the data structure to represent it.

Definition 1 Technology *defines the information that are related to the fabrication technology. It includes **LayerType** which is a set of mask types, **PlaneType** which is a set of plane types and a mapping from LayerType to PlaneType **PlaneMap** which is used to identify the plane that a polygon with certain mask type can stay on and **DesignRuleBase** which is used to store all the design rules specified by fabrication technology and will be discussed in more detail in Section 3.1.4.*

<i>Technology</i> = tuple {	1
$LayerType = \{space, ndiff, pdiff, poly, m1, m2, 2 \dots\};$	3
$PlaneType = \{active, m1, m2, poly, \dots\};$	4
$PlaneMap : LayerType \mapsto PlaneType;$	5
$DesignRuleBase : LayerType \times LayerType \mapsto \langle \rangle^{EdgeRule};$	6
}	7

Each polygon, also called a *tile*, is associated with a specific mask type as defined in Line 2. Tiles are linked by four pointers called *corner stitches*. Figure 3.2 gives an example of the tile structure in *metal1* plane. The pointer *l* at the lower left corner of a tile points to the direct left neighbor at the lower left corner of the tile. Pointer *b* at the lower left corner of a tile points to the direct bottom neighbor at the lower left corner of the tile. Similarly, pointers *t* and *r* at the upper right corner of a tile point to the upper neighbor and right neighbor of the tile, respectively. The coordinate $\{x,y\}$ is the position of the tile's lower left corner. The tile data structure is given in Definition 2. With the data structure for tile, the geometrical and physical characteristics of each tile can be fully determined from **Tile**. For example, given a tile *u*, the upper right coordinate, $(u.r.x, u.t.y)$, is decided by its right neighbor *u.r* and top neighbor *u.t* because the X coordinate of tile *u*'s right edge is also the X coordinate of the left edge of right neighbor *u.r* and Y coordinate of tile *u*'s upper edge is also the Y coordinate of lower edge of top neighbor *u.t*. Through tile *u*'s mask type *u.type*, the plane that *u* stays on can be obtained from function $PlaneMap(u.type)$. Thus the location and shape of each tile can be fully decided from Tile data structure.

Definition 2 Tile

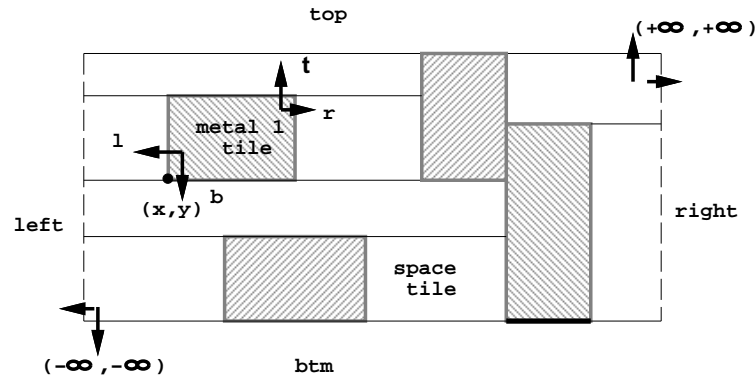


Figure 3.2: The tile structure in metal1 plane

<i>Tile</i> = tuple {	8
<i>type</i> : <i>LayerType</i> ;	9
<i>l, b, t, r</i> : <i>Tile</i> ;	10
<i>x, y</i> : \mathbb{Z} ;	11
}	12

Each plane is associated with a plane type as defined in Definition 1. A plane is composed of an ordered set of tiles. It extends from negative infinity to positive infinity. Four pseudo tiles *top*, *btm*, *left*, *right* are located at four boundaries of a layout. Any of these four pseudo tiles can be used as the starting tile for traversing a layout. The algorithms for traversing layout will be discussed in Section 3.1.3. The data structure for a plane is given in Definition 3.

Definition 3 Plane

<i>Plane</i> = tuple {	13
<i>type</i> : <i>PlaneType</i> ;	14
<i>tiles</i> : $\langle \rangle$ <i>Tile</i> ;	15
<i>top, btm</i> : <i>Tile</i> ;	16
<i>left, right</i> : <i>Tile</i> ;	17
}	18

Other than tiles and planes, layout designers tend to attach labels to certain signals. The data structure for label is given in Definition 4.

Definition 4 Label

<i>Label</i> = tuple {	19
<i>name</i> : <i>string</i> ;	20
<i>tile</i> : <i>Tile</i> ;	21
}	22

With the definitions for tile and plane, a layout can be formulated as a structure which includes a mapping from *PlaneType* to *Plane* and a set of labels as shown in Definition 5.

Definition 5 Layout

<i>Layout</i> = tuple {	23
<i>planes</i> : <i>PlaneType</i> \mapsto <i>Plane</i> ;	24
<i>labels</i> : $\langle \rangle$ <i>Label</i> ;	25
}	26

3.1.3 Algorithms

There are many algorithms used for processing tiles using corner stitching representation methodology defined in the previous section, such as neighbor tile finding, locating and enumerating tiles, searching area, etc [19]. This section gives a discussion of three algorithms often used in our migration engine.

Algorithm 1 *Find all the right neighbor tiles of given a tile s .*

```

rightNeighborFind = func(                                     27
    pl : Plane,                                              28
    s: Tile                                                  29
) : []Tile {                                               30
    var nbr : Tile;                                          31
    var nbrSet : []Tile;                                    32
                                                            33
    nbrSet =  $\emptyset$ ;                                       34
    nbr = ti.r;                                              35
    if( nbr  $\neq$  pl.right )                                  36
        do {                                               37
            nbrSet = nbrSet cup {nbr};                      38
            nbr = nbr.b;                                     39
        } while( nbr.y > s.y )                             40
    return nbrSet ;                                         41
}                                                            42

```

Example 1

Figure 3.3 shows an example to demonstrate this algorithm. The searching process is as follows:

1. First, it visits the top right neighbor of tile s through its \mathbf{r} pointer. If $s.r$ is not the right pseudo tile, add it into the neighbor tiles set.
2. Check if the bottom edge of the neighbor tile is still above the bottom edge of tile s . If this is true, move downward until it finds a tile whole bottom edge is lower than that of s .
3. Otherwise, return the neighbor tiles set.

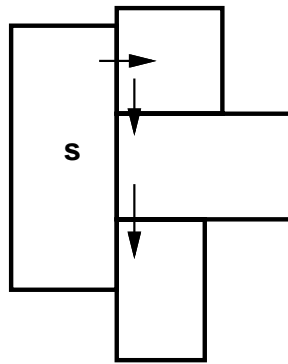


Figure 3.3: The process to find right neighbor tiles.

Algorithm 2 *Find the tile that contains a given (x,y) location on a given plane.*

```

searchTiles = func(                                     43
    layout : Layout,                                   44
    pl : Plane,                                       45
    x :  $\mathbb{Z}$ ,                                   46
    y :  $\mathbb{Z}$                                          47
) : Tile {                                           48
    var ti : Tile;                                    49
                                                    50
    ti = pl.top;                                       51
    if( y < ti.y )                                     52
        do ti = ti.b; while( y < ti.y ) ;           53
    else return ti ;                                   54
    if( y < pl.btm.u.y ) return ti ;                 55
    if( x > ti.r.x ) do {                             56
        ti = ti.r;                                     57
        while( ti.y > y ) ti = ti.b;                 58
    } while( x > ti.r.x )                             59
    return ti ;                                       60
}                                                    61

```

Here is an example to illustrate the process of finding the tile.

Example 2

Considering a simple layout in Figure 3.4, to find a tile that contains the point (x, y) , the algorithm starts from the *top* tile (tile 1) in the layout. The searching procedure is as follows:

1. First it checks whether y coordinate of the given point is beyond scope of the **top** tile or **btm** tile. If this is true, the tile that contains the given point is set to **top** tile or **btm** tile.

2. Otherwise, the search moves downward, until it finds the tile whose vertical range covers the desired point (For example, this occurs when tile 5 is found).
3. Select the right neighbor whose horizontal range contains the desired point and then trace rightward(For example, tile 6 has three neighbors: tile 7, tile 8 and tile 9. The lower bound of tile 7 and tile 8 is upper to the desired point, so it traces downward until tile 9 is found and from tile 9, trace goes rightward). The rightward trace keeps on until it finds the tile that contains the point (tile 10).

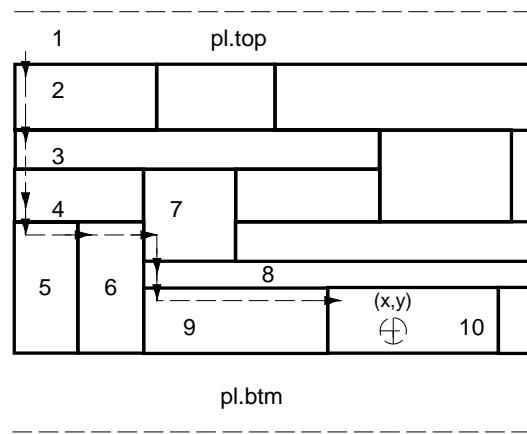


Figure 3.4: The process to locate the tile that contains a given point

Algorithm 3 *Enumerate all tiles on a given plane. In this algorithm, each tile is visited only after all tiles above it and to its left have been visited.*

```

enumerateTiles = func( pl : Plane ) : []Tile { 62
    var tiles : []Tile; 63
    var start : Tile; 64
    65
    tiles =  $\emptyset$ ; 66
    start = pl.top.b; 67
    while( start.b  $\neq$  pl.btm ) { 68
        tiles = eachTile( pl, tiles, start ); 69
        start = start.b; 70
    } 71
    return tiles ; 72
} 73
74

eachTile = func( 75
    pl : Plane, tiles: []Tile, ti: Tile 76
) : []Tile { 77
    var right : Tile; 78
    79
    tiles = tiles  $\cup$  {ti}; 80
    if( ti.r == NULL ) ; return tiles ; 81
    else { 82
        right = ti.r; 83
        while( right.y  $\geq$  ti.y ) { 84
            tiles = eachTile( pl, tiles, right); 85
            right = right.b; 86
        } 87
    } 88
} 89
90

```

Example 3

Figure 3.5 illustrates the algorithm. The process is as follows:

1. Start from the left most neighbor of the top tile at its bottom side in a given plane. Then step down through all the tiles at the left most side of the plane (the tiles with arrows inside in the figure).
2. For each tile in step 1, enumerate it recursively using the **eachTile** procedure given in lines from 1) to 4).
 - 1) Enumerate the tile.
 - 2) If the **r** stitch of the tile points to NULL, return from **eachTile** procedure (for example, when tile 2 is the current tile, tile 3 is its neighbor. But as tile 3 doesn't have any right neighbor, the procedure returns to the state when tile 2 is the current tile).
 - 3) Otherwise, visit all the tiles that touch the right side of the current tile (for example, when tile 13 is the current tile, visit tile 14 and tile 16).
 - 4) For each of these neighbors, if the **l** stitch points to the current tile, then call **eachTile** procedure to enumerate the neighbor recursively (for example, this occurs when tile 1 is the current tile and tile 2 is the neighbor).
3. The enumeration algorithm stops when it comes to the bottom tile of the plane.

3.1.4 Design Rule Modeling

The second input to migration tool is design rules. For IC designers, design rules are usually provided by manufacturers in the technology file. Each rule is explained by a simple English sentence with graphs illustrations to show the conditions in which the rule is applied. However, in order to be codified for use by migration tool, design rules need to be specified in an accessible and unambiguous format. There are two major methodologies for representing design

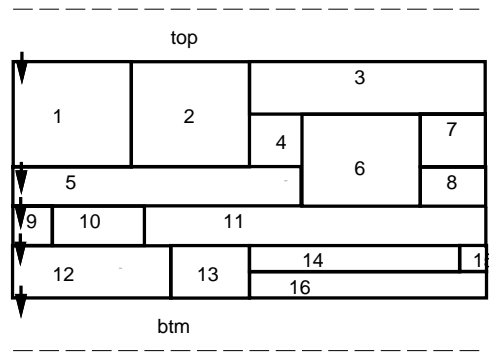


Figure 3.5: Tile enumeration.

rules. One is called *mask-based* design rule which is the basis of commercial design rule check package *Dracula* [2]; the other is called *edge-based* design rule model which is the basis of layout edit tool *Magic* [2]. In this project, the *edge-based* design rule model is used because of its ability to translate the high level design rules such as minimum spacing rule, minimum width rule, etc, into a set of edge rules and thus we can represent the design rules as constraints between individual edges. This section will briefly introduce this model and its data structure. For detailed discussion, please refer to [24].

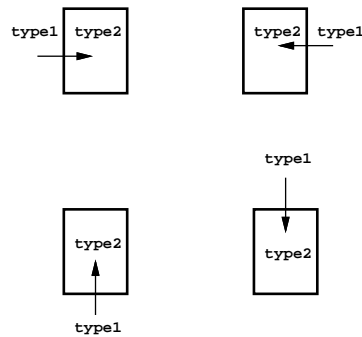


Figure 3.6: Each edge rule can be applied in any of the four directions.

The edge rule is applied on an edge between two tiles of different LayerType in any of four directions as shown by arrows in Figure 3.6. Without loss of generality, in the following discussion, we assume that the edge rule is applied towards the east. A distance *dist* and certain mask layers called *okTypes* area are specified so that only tiles of *okTypes* are permitted within

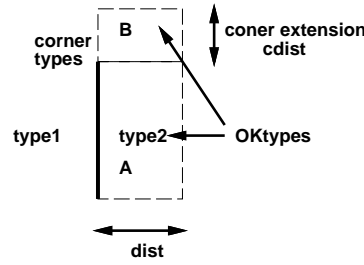


Figure 3.7: An example of edge rule.

the area A called *constraint region* as shown in Figure 3.7. In the corner region B, if the tile of type *cornerTypes* is just above and on the left of the edge, only *okTypes* tiles are allowed in area B. For simplicity, we call those tiles whose mask types do not belong to *okTypes* *forbidden tiles* for each edge rule. The constraint region can be on the same plane as the plane that tiles of type1 and type2 stay on, or any different planes as indicated in each edge rule.

The following data structure is used for modeling edge rules in the migration tool.

Definition 6 Edge rule.

<i>EdgeRule</i> = tuple {	91
<i>okTypes</i> : $\langle \rangle_{LayerType};$	92
<i>dist</i> : $\mathbb{Z};$	93
<i>cornerTypes</i> : $\langle \rangle_{LayerType};$	94
<i>cdist</i> : $\mathbb{Z};$	95
<i>flag</i> : $\langle \rangle_{\{area, rect, \dots\}};$	96
<i>plane</i> : <i>PlaneType</i> ;	97
}	98

Given a pair of *LayerType*, a set of edge rules can be accessed through *DesignRuleBase* defined in *Technology*.

3.2 Migration Engine

As the layout is composed of a set of tiles, the migration engine can generate a new layout by determining new positions of horizontal and vertical edges of all tiles. It employs the traditional 1-D compaction strategy by first migrating along the X direction, i.e. determining positions of vertical edges, and then the Y direction. Without loss of generality, in the discussion that follows, we assume migration in the X direction only.

The basic strategy for migration is to abstract all the requirements or constraints among all the edges in a layout, such as design rules and other practical consideration. And then with respect to all these constraints, new edge positions are decided under certain optimization goal. With the corner stitching data structure discussed in Chapter 2, tile shapes and design rules are specified in the Mead and Conway's λ based methodology [16], which means that the positions of tiles are all specified in terms of λ . Take the layout in Figure 3.8, tiles are all aligned in grids whose minimum spacing is 1λ , which implies that the coordinates of all edges are integers. At the same time, design rules are specified in terms of λ also. And all design rules can be expressed as inequalities when they are applied to the layout. For example, suppose the minimum width requirement for tile 1 is 4λ in Figure 3.8 and this rule can be translated into an inequality as:

$$x_2 - x_1 \geq 4 \tag{3.1}$$

Thus, the layout migration problem can be formulated as an integer linear programming (ILP) problem:

$$\begin{aligned} & \text{minimize} && o^T x \\ & \text{subject to} && Ax \geq b \\ & && x \geq 0 \end{aligned}$$

Here x is a vector of variables to be determined, and in the simplest case would just be

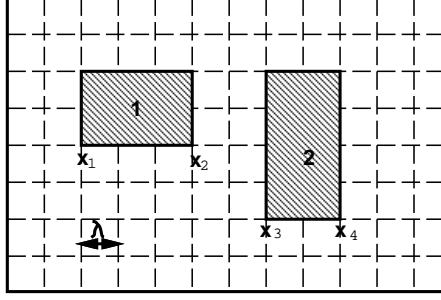


Figure 3.8: Tiles are aligned in grids

coordinates for all vertical edges. In this project, x is a vector of coordinates for all tiles' left vertical edges. Vectors o represent the coefficients of x in the objective function of optimization. Each row of array A represents coefficients of x in an inequality. We call this type of migration as *constraint-based migration*.

Suppose we want to migrate the layout in Figure 3.8 so that the new layout does not have design rule violations and the layout area is minimum. For simplicity, we only consider the minimum width rule and minimum spacing rule for tile 1 and tile 2. The minimum width for tile 1 and tile is 4λ and minimum distance between tile 1 and tile 2 is 3λ . This problem is formulated as:

$$\begin{aligned}
 & \text{minimize} && x_4 - x_1 \\
 & \text{subject to} && x_2 - x_1 \geq 4 \\
 & && x_4 - x_3 \geq 4 \\
 & && x_3 - x_2 \geq 3 \\
 & && x_1 \geq 0 \\
 & && x_2 \geq 0 \\
 & && x_3 \geq 0 \\
 & && x_4 \geq 0
 \end{aligned}$$

After solving this ILP problem, we can get the value for each x , and new positions of each

edge can be obtained as shown in Figure 3.9.

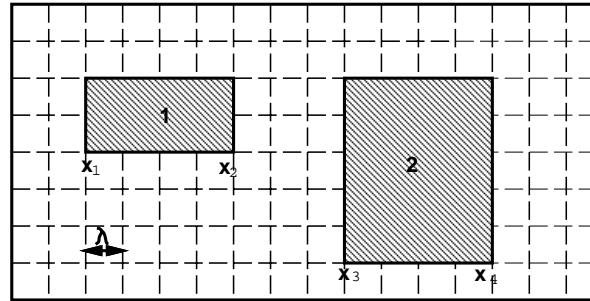


Figure 3.9: Each tile has new position and shape after migration with no design rule violations.

Section 3.3 will discuss how to translate the design rules requirements into inequalities in 3.2, so called constraints, so that the generated layout is design rule clean. In addition, three goals to optimize the migrated layout are compared in section 3.4 and a brief discussion of ILP solver is also provided at the end of this chapter.

3.3 Design Rule Constraint Generation

The design rule constraint generation is used to generate the distance requirements of every pair of edges according to design rules so that the migrated layout does not have design rule violations. This section will discuss how to generate these constraints according to the edge rules specified by the technology.

3.3.1 Design Rule Checking

The design rule constraint generation process is very similar to design rule checking. Before the discussion of design rule constraint generation, we can first look at how design rule checking works.

To check a region, the design rule checker first searches all tiles in the plane. For each tile, the checker examines all the neighbors along one side. As the tile may have more than

one neighbor that are of different mask types. A design rule checker divides the tile's side into several edges that has only one with one material on each side. When processing the edge, checker uses the mask types of tiles at each side of the edge as the index into the design rule database to find the edge rule $r : EdgeRule$ that can be applied on that edge. Then, design rule checker searches within the constraint region for tiles whose mask type don't belong to $r.okTypes$ as shown in Figure 3.10. The plane that a constraint region stays on can be on either the plane that the edge being processed stays on or another plane which is decided by $r.plane$. In the next section, we will look at the *IntraPlane checking* process where the constraint region stays on the same plane as the tile processed. Section 3.3.5 will discuss the *InterPlanechecking* process where checker needs to jump to another plane to look for forbidden tiles.

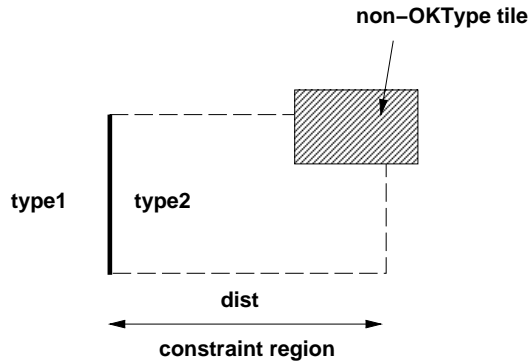


Figure 3.10: Design rule checker looks for non-OKType tiles within constraint region.

3.3.2 IntraPlane Design Rule Constraint Generation

Design rule constraint generation can take similar procedure as design rule checking discussed in previous section, except that the searching region should go beyond constraint region specified by design rules. The reason is that migration assumes that every tile has the potential to move, which means those forbidden tiles that are not inside constraint region in the original layout may move into constraint region after migration. An intuitive way to avoid missing con-

straints is to extend the constraint region to the boundary of layout as the checking region in Figure 3.11(a) and generate constraints between all necessary pair of edges. Take poly spacing rule as an example, the TSMC $0.25\mu m$ technology specifies that the spacing of poly should be greater than 3λ , which can be translated into edge rule as the following:

edge *poly* $\overline{\text{poly}}$ 3 $\overline{\text{poly}}$ 3

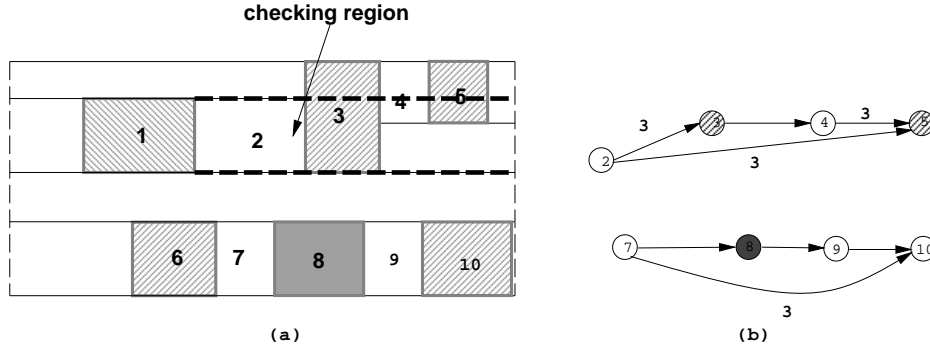


Figure 3.11: (a) An example layout in active plane. The shaded rectangles 1, 3, 5, 6 and 10 represent poly tiles. Rectangle 8 is diffusion tile. Other rectangles are all space tiles. (b) The constraint graph generated from poly spacing rule.

Given a simple layout as Figure 3.11(a), according to this rule, four constraints need to be generated to guarantee enough spacing between poly when processing the edge between tile 1 and tile 2 (corner region checking is not considered at this moment). They are:

- $x_3 - x_2 \geq 3$ The left edge of tile 3 should be at least 3λ away from left edge of tile 2.
- $x_5 - x_2 \geq 3$ The left edge of tile 5 should be at least 3λ away from left edge of tile 2.
- $x_5 - x_3 \geq 3$ The left edge of tile 5 should be at least 3λ away from left edge of tile 3.
- $x_{10} - x_7 \geq 3$ The left edge of tile 10 should be at least 3λ away from left edge of tile 7.

These constraints can be visualized using a directed graph $G = \langle V, E \rangle$ as shown in Figure 3.11(b). Each vertex represents the X coordinate of a tile's left edge. For each inequality of the form $x_j - x_i \geq d_{ij}$, there is an arc $\langle v_i, v_j \rangle$ with weight d_{ij} .

Note that with constraint-based migration methodology, the width and height of tiles may be changed after migration in order to satisfy the constraints. However, migration must maintain that the given circuit topology keep the same functionality of the circuit, i.e., the corner stitching representation of the layout is kept unchanged. So after migration, the four pointers of each tile must point to the same tiles as in the old layout. The relative position of tiles are not changed. For example, the tile 5 in Figure 3.11 is on the right side of tile 3 in the old layout and after migration tile 5 cannot move to the left side of tile 3. Therefore, the arc $\langle v_2, v_5 \rangle$ in Figure 3.11(b) is redundant because the tile 5 is always on the right side of tile 3 and the distance constraint between left edge of tile 2 and tile 3 (arc $\langle v_2, v_3 \rangle$) guarantees that the distance between left edge of tile 2 and tile 5 cannot be less than 3λ . In other words, if an edge of forbidden tile (tile 5) stays behind another forbidden tile (tile 3), it will not generate constraint between the edge that is being processed and the edge in the “shadow” of forbidden tiles.

Another redundant arc in Figure 3.11(b) is arc $\langle v_7, v_{10} \rangle$. As discussed before, the tile structure will not be changed after migration, which implies that tiles cannot be eliminated after migration. We can assume that the minimum tile width should be greater than or equal to 1λ . So the minimum separation between the left edge of tile 7 and tile 10 should be greater or equal than the sum of minimum width requirement of tile 7, 8 and 9, which is greater than or equal to the minimum spacing 3λ . This makes the arc $\langle v_7, v_{10} \rangle$ redundant for migration.

A new design rule constraint generation method *Depth-K searching* algorithm is proposed in this project which greatly reduces the checking region and reduces the redundant constraints. A detailed discussion of this algorithm follows.

3.3.3 The Depth-K searching algorithm

To gain more insight into the problem, we first build a graph *shadowing neighborhood graph* that captures the neighboring relation. As we can observe from Figure 3.11 that constraints should be generated only for tiles that overlap with the checking edge vertically, a *shadowing neighborhood graph* defined in Definition 7 is used to limit the searching space.

Definition 7 Given a tile called *source tile* in a plane, its shadowing neighborhood graph $N = \langle V, E^N \rangle$ is a directed graph whose vertices correspond to the tiles that overlap with the source tile in the Y direction, and an edge $\langle u, v \rangle \in E^N$ iff tile u and v share a common edge.

While the shadowing neighborhood graph is effective limiting the search space in the Y direction, we propose a new strategy to further limit the searching space in X direction. We observe that as we explore along the X direction, each tile has a minimum width requirement dictated by the design rule or by topology keeping requirement. This can be summed up along the path and be used as the bottom bound estimate of the distance between the source tile and the current tile. Let's assume D is the maximum *dist* value among all the edge rules. If the lower bound exceeds the constraint distance D , further exploration of the current tile can be stopped.

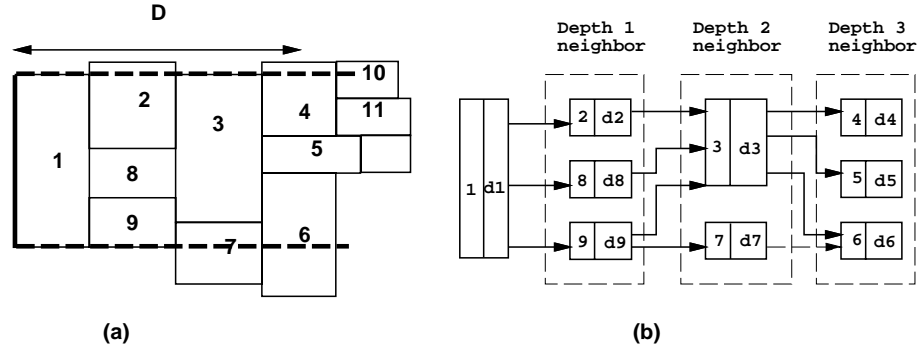


Figure 3.12: (a) A fraction of a layout plane. Tile 1 is the source tile that is being processed for edge rule constraint generation. (b) Depth-K shadowing neighborhood graph for tile 1.

Example 4 Consider the layout example in Figure 3.12 (a). The shadow is indicated by the dashed line. A fraction of the neighborhood graph is shown in Figure 3.12(b), where each tile is labeled with its minimum width requirement of d_1, d_2 etc. Suppose the constraint distance is D , and $d_1 + d_2 + d_3 \leq D$, $d_1 + d_2 + d_3 + d_4 \geq D$, then tile 10 and tile 11 will be pruned from the searching space.

As such, it is guaranteed that there exists an upper bound of the depth we have to search. We denote the maximum number of depths as K , which is totally decided by the design rules. Given K , the definition of Depth- K shadowing neighborhood graph is given in Definition 8 and Algorithm 4 shows how it is built.

Definition 8 *Given a shadowing neighborhood graph $N = \langle V, E^N \rangle$, its **Depth- K shadowing neighborhood graph** is a directed graph $\overline{N} = \langle V, \overline{E^N} \rangle$ such that $\langle u, v \rangle \in \overline{E^N}$ iff $\exists p \in u \rightsquigarrow v. |p| \leq K$ and $[u.y, u.t.y] \cap [v.y, v.t.y] \neq \emptyset$.*

Algorithm 4 *Depth- K searching algorithm.*

```

input:  $s : \text{Tile};$  99
         $pl : \text{Plane};$  100
         $r : \text{EdgeRule};$  101
output:  $\overline{N} = \langle V, \overline{E^N} \rangle;$  102
func  $\text{depthKShadowingClosure}()$  { 103
     $V = \{s\};$  104
     $\overline{E^N} = \emptyset;$  105
    forall(  $u \in \text{rightNeighborFind}(pl, s)$  ) { 106
         $\text{explore}(s, u, 1);$  107
    } 108
} 109
func  $\text{explore}(u, v, \text{depth})$  { 110
    if(  $[s.y, s.t.y] \cap [v.y, v.t.y] = \emptyset \vee \text{depth}++ > K$  ) 111
        return; 112
     $\overline{E^N} = \overline{E^N} \cup \langle u, v \rangle;$  113
     $V = V \cup \{v\};$  114
    if(  $v.\text{type} \notin r.\text{okType}$  ) 115
        return; 116
    forall(  $w \in \text{rightNeighborFind}(pl, v)$  ) 117
         $\text{explore}(v, w, \text{depth});$  118
    } 119

```

After Depth-K shadowing neighborhood graph is built, design rule constraints for source tile s can be added to constraint graph $G = \langle V, E \rangle$ by traversing its Depth-K shadowing neighborhood graph $\overline{N} = \langle V, \overline{E^N} \rangle$. Algorithm 5 shows how the design rule constraint are generated when given the Depth-K shadowing neighborhood graph.

Algorithm 5 *Edge rule constraint generation.*

```

input:  $s : \text{Tile};$  120
 $\overline{N} = \langle V, \overline{E^N} \rangle;$  121
 $R : \text{EdgeRule};$  122
output:  $G = \langle V, E \rangle;$  123
func addEdgeConstraints() { 124
  forall(  $u \in V$  ) 125
    if(  $u.type \notin R.OKType$  ) { 126
       $E = E \cup \langle s, u \rangle;$  127
       $weight(\langle s, u \rangle) = R.dist;$  128
    } 129
  } 130
} 131

```

To analyze the complexity of *Depth-K searching* algorithm, we assume that the total number of tiles in a layout is N . For any source tile s , the best case for the *Depth-K searching* algorithm is for a row of tiles to sit beside s as shown in Figure 3.13. In this case, this algorithm would process K tiles for s . The worst case is shown in Figure 3.14 where s has $N - 1$ neighbors and $N - 1$ tiles need to be processed for s . From the experimental result given in Section 5.2.1, the expected time complexity of the whole design rule constraint generation process is $O(N^{1.4})$, which includes both time cost for tile enumeration algorithm and *Depth-K searching* algorithm.

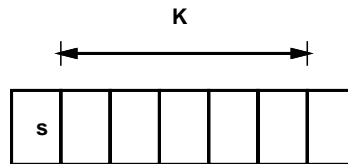


Figure 3.13: The best case for Depth-K searching algorithm

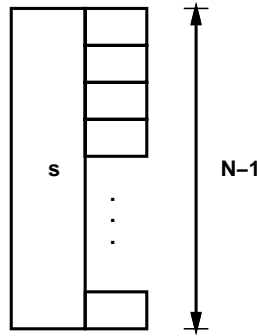


Figure 3.14: The maximum number of tiles to be visited for tile s

Figure 3.15 and 3.16 gives an example of IntraPlane design rule constraints generated for leaf cell *muxf201*. The constraint graph is visualized in Figure 3.16.

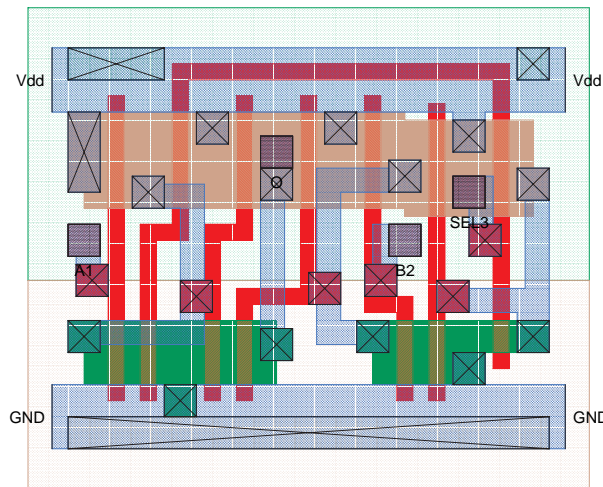


Figure 3.15: A leaf cell muxf201.

3.3.4 Corner checking and Interpass constraint generation

In addition to the design rule constraints in the constraint region, edge rule also specifies the corner region of an edge that needs to be examined as shown in Figure 3.17(a). The shape of corner region is a $cdist \times dist$ rectangle. As every tile has the potential to move, the constraint generation should also search beyond the corner constraint region. The Depth-K searching

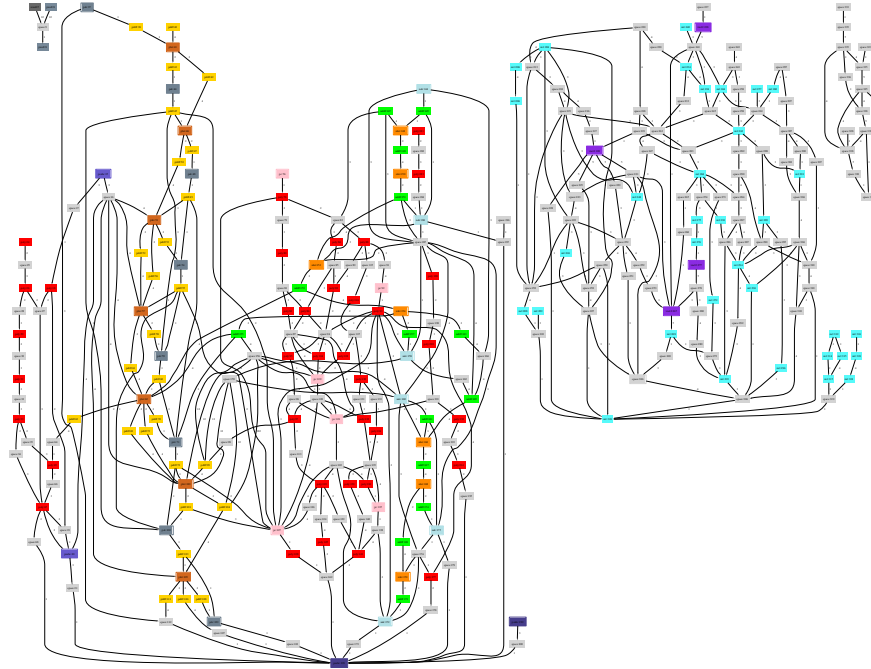


Figure 3.16: The constraint graph for IntraPlane constraints.

algorithm can be applied to constraint generation in the corner region also. The only difference is that in the Y direction, the searching should proceed to the K^{th} neighbor tile as shown in Figure 3.17(b). As this algorithm is very similar to the Depth-K searching algorithm, we will not give a detailed description of it.

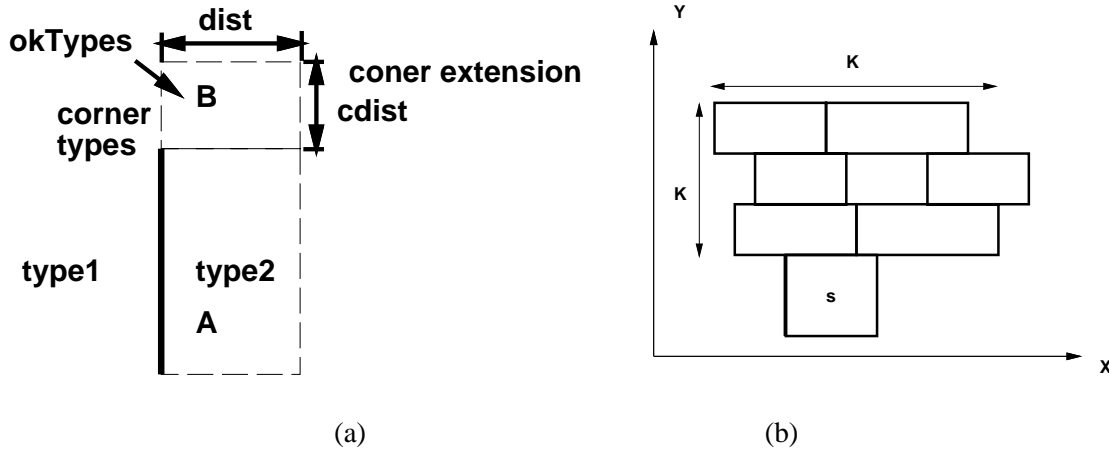


Figure 3.17: Corner constraint region checking

As we employ the traditional 1-D migration, X migration and Y migration are independent of each other, which may give rise to missing constraints for both X migration and Y migration.

Example 5 *Considering the layout in Figure 3.18, let's suppose that tile 3 is located above the constraint searching region and it is not included in the Depth-K shadowing neighborhood graph. So, during X direction migration no constraint is generated between left edge of tile 1 and left edge of tile 3. After X direction migration and Y direction migration, it is possible that tile 3 moves into area A. A design rule violation may occur if the distance between left edge of tile 3 and left edge of tile 1 is less than the distance requirement from edge rule.*

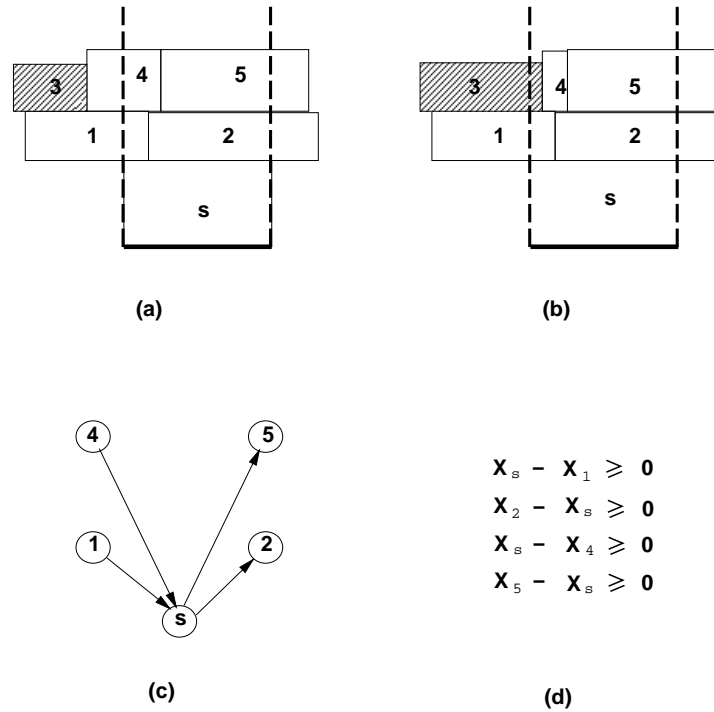


Figure 3.18: (a) In the old layout, tile 3 doesn't overlap with tile s in X direction. (b) After X direction migration and Y direction migration, tile 3 moves into shadow area of tile 1. (c) Interpass Constraint graph for tile s (d) Interpass constraints for tile s.

To solve this problem, additional constraints called *interpass constraints*, need to be generated to prevent the arbitrary movement of tiles during X and Y direction migration. Take the

layout in Figure 3.18(a) for example, given a source tile s , for each tile that overlaps the left boundary of tile s in the X direction such as tile 1 and tile 4, we generate constraints between the left edge of tile s and both vertical edges of tile 1 and tile 4 to guarantee that the left edge of s stays within tile 1 and tile 4 as illustrated in Figure 3.18(c,d). With interpass constraints, those tiles that do not overlap source tile in the original layout will always be kept away from checking area, thus no new design rule violations will occur after migration.

Algorithm 6 *Interpass Constraint Generation*

input: $s : \text{Tile};$	132
$\overline{N} = \langle V, \overline{E^N} \rangle;$	133
output: $G = \langle V, E \rangle;$	134
func <i>InterpassConstraints()</i> {	135
forall ($u \in V$)	136
if ($s.x \in [u.x, u.r.x]$) {	137
$E = E \cup \langle u, s \rangle;$	138
$weight(\langle u, s \rangle) = 0;$	139
$E = E \cup \langle s, u.r \rangle;$	140
$weight(\langle s, u.r \rangle) = 0;$	141
}	142
}	143

3.3.5 InterPlane Constraint generation

Other than the constraints between tiles on the same plane, edge rules also specify the distance requirements between tiles on different planes, indicated by the value of *plane* in each edge rule. For example, the minimum spacing requirement between N-well and pdiffusion in TSMC $0.25\mu\text{m}$ technology is 6λ . However, Well tiles and active tiles are in different planes in the

corner stitching layout representation as shown in Figure 3.21. So the value of *plane* in this edge rule given in is set to *active* as shown below:

edge *space* $N - well$ \overline{pdiff} 6 \overline{pdiff} 6 **active**

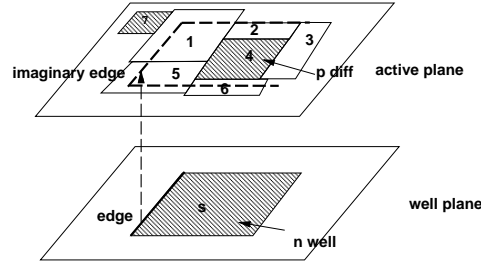


Figure 3.19: N-well tile stays on well plane while diffusion tile stays on active plane.

The Depth-K searching algorithm is modified slightly to be applied for interplane constraint generation. For intraplane constraint generation, the Depth-K shadowing neighborhood graph is built on the same plane as the plane that the source tile *s* stays on and the constraint region starts from the edge of tile *s*. However, for interplane constraint generation, the Depth-K shadowing neighborhood graph is built on checking plane as indicated in the edge rule. We first map the edge being processed to an imaginary edge on the checking plane as shown in Figure 3.21. The imaginary edge has exactly the same length and location as the edge being processed. Then the Depth-K shadowing neighborhood graph can be built with Depth-K searching algorithm on the checking plane. The Depth-K shadowing neighborhood graph for layout in Figure 3.21 and the corresponding interplane edge rule constraint are given in Figure 3.20.

However, for interplane edge rules, the constraints generated above are not enough to guarantee that validity of the migrated layout. The main reason is that the movement of tiles in different plane are independent if no further constraints are generated, which may cause design rule violations in the migrated layout. For example, if no constraints between the left edge of tile 1 in Figure 3.21 and that of source tile *s*, the tile 7 which is also a P-diffusion tile may move to the right of edge and the distance may be within 6λ , which will cause design rule

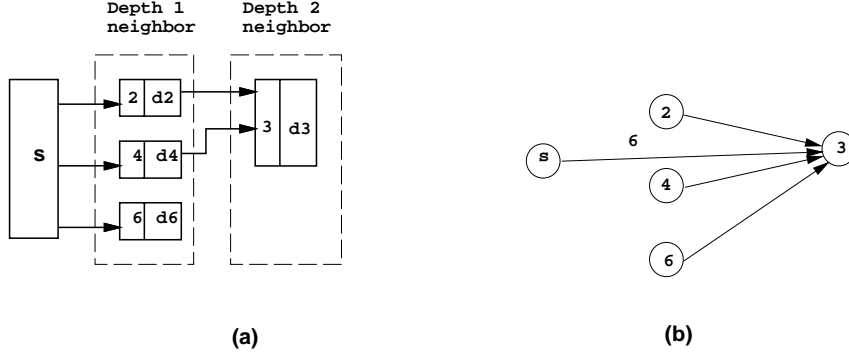


Figure 3.20: (a)The Depth-K shadowing neighborhood graph for interplane edge rule (b) InterPlane edge rule constraint between source tile s and tile 3.

errors. Also, tile 4 may also move outside of the constraint region which makes constraints between tile s and tile 3 unnecessary. So two more types of constraints need to be generated with the interplane design rule.

- InterPass constraints in the X direction for interPlane edge rule. This set of constraints is used to guarantee that the imaginary edge of source tile s still overlap's with the same tiles in the old layout. Given the layout in Figure 3.21, we will generate constraints:

$$\begin{aligned}
 x_s - x_1 &\geq 0 & x_s - x_2 &\leq 0 \\
 x_s - x_5 &\geq 0 & x_s - x_4 &\leq 0 \\
 x_s - x_6 &\leq 0
 \end{aligned} \tag{3.2}$$

With these constraints, the relative position in the X direction of those tiles in different planes will be kept unchanged. Therefore, forbidden tiles such as tile 7 on the left side of the imaginary edge will not move to the right side of it after migration and vice versa. Otherwise, the new layout may have design rule violations between the source tile and forbidden tile that were not considered in Depth-K shadowing neighborhood graph.

- InterPass constraints in the Y direction for interPlane edge rule. It is very similar to interpass constraints for intraPlane edge rule, except that source tile is in different plane.

For the layout in Figure 3.21, we need to generate constraints for the bottom edge of tile s to guarantee that after migration, the bottom edge of tile s still overlaps with tiles that overlapped with it in the original layout:

$$y_s - y_5 \geq 0 \quad y_s - y_1 \leq 0$$

$$y_s - y_6 \geq 0 \quad y_s - y_4 \leq 0$$

The constraints for top edge of tile s can be built in the same way. With this set of constraints, the forbidden tiles in the checking plane will still stay within the constraint region after migration. Other forbidden tiles that were above or below the constraint region will be kept away from the constraint region so that no new violation will occur after migration.

Figure 3.21 shows a real example of InterPlane constraints generated for leaf cell muxf201 given in Figure 3.15.

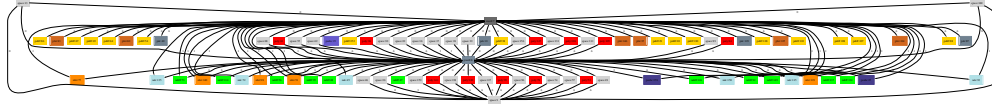


Figure 3.21: InterPlane constraints generated for cell muxf201.

3.3.6 Connect Constraints Generation

Connect constraints are generated to guarantee the correct presentation of contact tiles after migration. As we know from Chapter 2, corner-stitching partitions the mask layers into separate planes. Layers that overlap may cause electrical constructs to be partitioned into the same plane. Those layers that overlap with little electrical significance will be partitioned into different planes [22]. For example, polysilicon, diffusion, and their overlaps (transistors) are stored in **active** plane, while metal1 that does not interact with these layers is stored in a different plane, **metal1** plane.

However, because the **contact** mask type connects layers in different planes, it is a special case. It has to be represented in all planes that it connects. In the technology file, contact is specified in a Contact section with specialized syntax. An example of polycontact is shown below:

```
contact
pcontact      poly      metal1
end
```

The contact declaration begins with a contact type called *base type*. In this example, pcontact is a base type for polycontact. The remainder of this declaration is a list of non-contact mask types (poly and metal1 in the example) that are connected by this contact. These types are referred to as *component* type of the contact. The home plane of the first component type will be the home plane for contact and contact also has an *image* tile type on the planes where other component type tiles stay. For example, pcontact's home plane is active plane which is also the home plane for poly. A pcontact has a image tile type *pdcontact/metal1* that is stored in metal1 plane as illustrated in Figure 3.22.

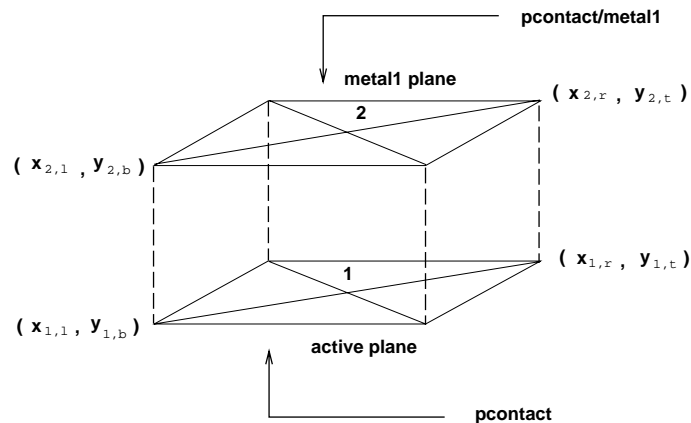


Figure 3.22: A contact has different tile types on the planes it connects. The poly contact in this figure has **pcontact** tile (tile 1) on active plane and **pcontact/metal1** tile (tile 2) on metal1 plane.

Although a contact has two tile copies using the corner stitching representation, the contact still represents **one** via hole in physics. So, the base tile and image tile of a contact should have exactly the same shape and stay at the same location on the component planes. Given a layout for migration, the corner stitching data structure itself has no mechanism to guarantee this requirement. Therefore, we generate four equalities called *connect constraints* for this requirement to guarantee that base type tile and image type tile of a contact are exactly the same after migration. For example, for the poly contact in Figure 3.22, we will generate:

$$x_{1,l} = x_{2,l}$$

$$x_{1,r} = x_{2,r}$$

$$y_{1,b} = y_{2,b}$$

$$y_{1,t} = y_{2,t}$$

Figure 3.23 shows a real example of Connect constraints generated for leaf cell muxf201 given in Figure 3.15.



Figure 3.23: Connect constraints generated for cell muxf201.

3.4 Objective function

After constraints are generated, the migration engine needs to build an objective function according to the kind of optimization goal the user wants to achieve and dump both the constraints and objective function to the ILP solver. The new positions of each tile will be determined from the ILP solver. The performance of the migrated layout is largely influenced by the choice of objective function. In this section, we discuss three objective functions and their impacts on layout.

3.4.1 Minimum area objective function

The traditional minimum layout area objective function takes the layout area as the criteria and shrinks area to a maximum extent. Given a layout in Figure 3.24, the minimum layout objective function will be formulated as:

$$\text{minimize } x_r - x_l \quad (3.3)$$

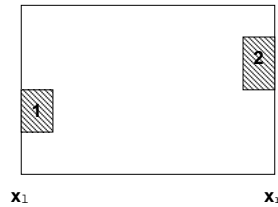


Figure 3.24: Tile 1 is the leftmost tile in a layout and x_l is the X coordinate of its left edge. Tile 2 is the rightmost tile in the layout and x_r is the X coordinate of its right edge.

However, one of the disadvantages of the minimum area objective function is that this criterion tends to shrink the layout recklessly without considering layout design issues. There exist some circumstances that increasing the layout area a little bit would be beneficial to circuit performance and chip yield. For example, power lines in the layout are usually designed to be wide instead of narrow to minimize the electromigration and resistance effects. Also, layout designers tend to make space between two important signals to minimize the coupling between them. As the minimum area objective function cannot take care of these issues, we introduce the *minimum perturbation* and *geometric closeness* objective functions in the following sections.

3.4.2 Minimum perturbation objective function

In order to take full advantage of the original design and make minimum changes to the migrated layout, the *Minimum perturbation* objective is proposed in [10], which is defined as:

$$\text{minimize} \quad \sum |x - x^{old}| \quad (3.4)$$

where x is the vector of variables that determine X coordinates of all vertical edges and x^{old} is the vector of constants that are the original X coordinates of all vertical edges in the layout. The minimum perturbation function minimizes the position changes of all edges and snaps the edges to their original positions as much as possible. However, the disadvantage of this function is that it minimizes the absolute coordinates of edges and will penalize more on the movement of edges on the right side of the layout.

Example 6 Consider a simple layout given in Figure 3.25 with two tiles of metal2 type. Because of technology change, the minimum width requirement of tile 1 is changed from 4λ to 5λ and the distance requirement between tile 1 and tile 2 is changed from 4λ to 5λ too. Based on minimum perturbation objective function, the layout will be migrated to the one on the lower part of Figure 3.25. The right edge of tile 1 will be stretched rightward by 1λ and left edge of tile 2 will be moved rightward by 2λ . However, the right edge of tile 2 stays at the old position because without change of its position, its width is 5λ which satisfies the new design rule. Otherwise, the objective function value will be greater than the one with x'_2 unchanged.

It can be seen from this example that the movement of edges on the left side will add penalties on the edges on the right side if we want to preserve the original shape of tiles on the right.

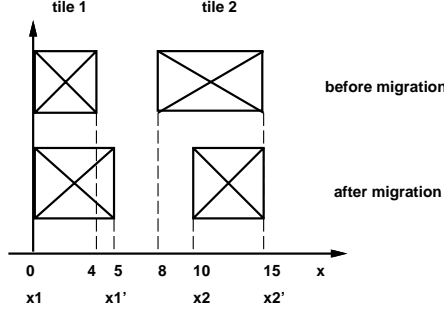


Figure 3.25: The old layout and migrated layout with minimum perturbation objective function.

3.4.3 Geometric closeness objective function

To remove this penalty, a new objective function, *geometric closeness* objective function is introduced which is defined as :

$$\text{Minimize } \sum |(x_{ri} - x_{li}) - (x_{ri}^{old} - x_{li}^{old})| \quad (3.5)$$

Here, x_{ri} and x_{li} are the X coordinates of the right and left edges of each tile in the layout. The constants x_{ri}^{old} and x_{li}^{old} are the X coordinates of the right and left edges of the corresponding tile in the original layout. Instead of minimizing the absolute coordinate changes of edges, this function minimizes the shape changes of all tiles so that each tile change will not add penalty to other tiles.

To linearize, or to remove the absolute value computation in Equation (3.5), we use a method similar to [10] by introducing two variables R_i and L_i for each tile, such that Equation (3.6) are introduced as constraints,

$$\begin{aligned} R_i &\geq x_{ri} - x_{li} \\ R_i &\geq x_{ri}^{old} - x_{li}^{old} \\ L_i &\leq x_{ri} - x_{li} \\ L_i &\leq x_{ri}^{old} - x_{li}^{old} \end{aligned} \quad (3.6)$$

and the objective function is replaced by Equation (3.7):

$$\text{Minimize } \sum (R_i - L_i) \quad (3.7)$$

Equation (3.7) and Equation (3.5) is equivalent for this ILP problem and the proof is given in the following:

Proof:

$$\text{From constraints : } R_i \geq x_{ri} - x_{li} \quad \text{and} \quad R_i \geq x_{ri}^{old} - x_{li}^{old}$$

$$\text{we get} \quad R_i \geq \max\{(x_{ri} - x_{li}), (x_{ri}^{old} - x_{li}^{old})\}$$

$$\text{Similarly,} \quad L_i \leq \min\{(x_{ri} - x_{li}), (x_{ri}^{old} - x_{li}^{old})\}$$

Because for any i , $(R_i - L_i)$ has the minimum value only when $R_i = \max\{(x_{ri} - x_{li}), (x_{ri}^{old} - x_{li}^{old})\}$ and $L_i = \min\{(x_{ri} - x_{li}), (x_{ri}^{old} - x_{li}^{old})\}$, we get:

$$\begin{aligned} & \min\{ \sum (R_i - L_i) \} \\ &= \min\{ \sum (\max\{(x_{ri} - x_{li}), (x_{ri}^{old} - x_{li}^{old})\} - \min\{(x_{ri} - x_{li}), (x_{ri}^{old} - x_{li}^{old})\}) \} \\ &= \min\{ \sum |(x_{ri} - x_{li}) - (x_{ri}^{old} - x_{li}^{old})| \} \end{aligned}$$

□

Example 7 With the geometric closeness objective function, the example given in Figure 3.25 will be migrated into the layout in Figure 3.26. It can be seen that the width of tile 2 is set to the original value and the topology of the old layout is preserved to a maximum extent.

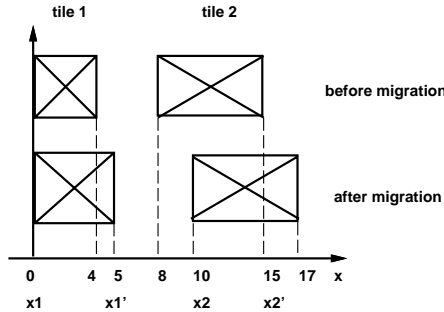


Figure 3.26: The old layout and migrated layout with geometric closeness objective function.

3.5 Integer Linear Programming Solver

With all the constraints and the objective function generated, an integer linear programming solver is needed to get the optimized solution for each variable. For all the test libraries, including the datapath library and the standard cell library, there will be up to 2,000 variables and 40,000 constraints (shown in Appendix A and B). We use the free ILP solver, called *lp_solve*, by Michel Berkelaar from Northwestern University and Argonne National Laboratory. (<http://www.cs.sunysb.edu/algorithm/implement/lpsolve/implement.shtml>). The program can solve the ILP problem with as many as 30,000 variables and 50,000 constraints, which fits our requirement. We can get a design rule clean layout after we assign the new position of each tile from the result generated by ILP solver.

Chapter 4

Migration for datapath and standard cell libraries

The migration engine described in Chapter 3 can migrate a layout to new technology without design rule violations. However, it is not enough to handle migrating a library of leaf cells. Today's ASIC design flow prerequisites the existence of library of cells that can be used for synthesis or place & route tools. The total design is built from assembling these leaf cells in the library. The design of leaf cells has more issues to consider so that they are compatible with the synthesis or Place & Route tools. In this chapter, we will explore the *overall library architecture* requirements for datapath and standard cell libraries and how these requirements are solved using our migration engine.

4.1 Datapath library migration

In digital signal processing (DSP) ICs and microprocessors, the datapath is the core where all computations are performed. A system's performance is largely determined by the design and implementation of its datapath. A datapath consists of interconnection of basic combinational functions, such as logic (AND, OR) or arithmetic operators (addition, multiplication, com-

parison). In this project, we call these functions or operators *function blocks*. One of the most important characteristics of datapath cells is that there are several buses of data flowing through the function block at the same time. An example circuit given in Figure 4.1 shows two 8-bit signals flowing through an 8-bit adder and produce the output O.

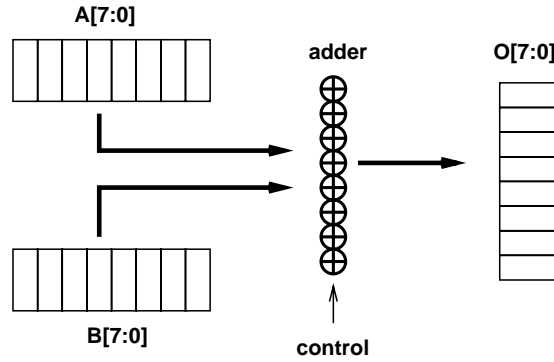


Figure 4.1: An 8-bit adder block diagram.

As we can see from Figure 4.1, the adder for each signal bit is identical. In order to reduce wire lengths and increase the layout density, designers can use *structured custom design* and build an N-bit function block by abutting predesigned leaf cells as shown in Figure 4.2. However this design approach is based on the fact that leaf cells must be carefully designed to fit into this structure. For example, the control signals in the 8-bit adder in 4.2 must align vertically, so that when the leaf cells are tiled, these lines are contiguous.

Figure 4.3 shows the leaf cell layout structure of the one bit cell in datapath library [3]. This is considered a typical datapath leaf cell.

We can observe from Figure 4.3 some important characteristics about a datapath leaf cell:

- Power rails run vertically in metal1 and cover the entire cell in the Y direction so that power lines are contiguous when cells are abutted. The width of power line is specified by the designer and the spacing is variable.
- There are signal ports other than power rails to allow abutment. Mostly, these signals are control signals for each bit cell. The width and spacing of these signal ports are variable.

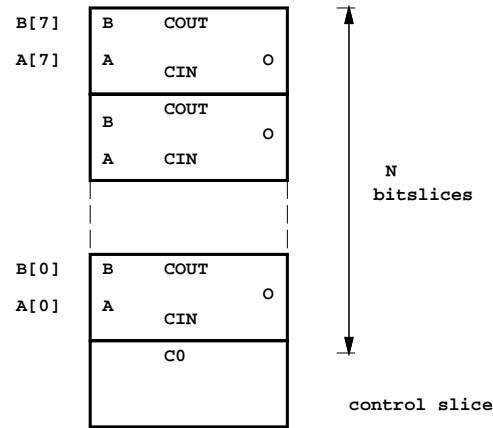


Figure 4.2: An 8-bit adder constructed by abutting 8 adder bitslices and 1 control slice.

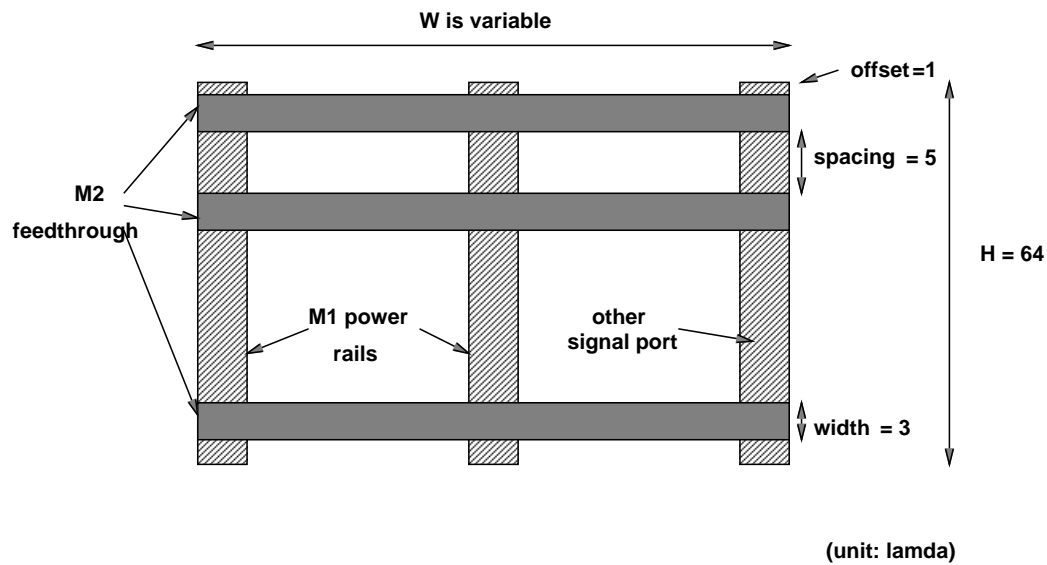


Figure 4.3: An example of datapath library cell.

- There are horizontal feedthroughs implemented on metal2 for connection of I/O ports between different function blocks. The width, spacing and offset of feedthroughs are decided by designers.

The following section will discuss how we model each of these function block architecture requirements into constraints so that the migrated leaf cells can be used the same way before migration.

4.1.1 Port matching

As we can see from Figure 4.2, the area efficiency in the datapath is achieved by the *tiling* strategy where important signals, such as Vdd/Gnd and controls, are implicitly routed by abutment. This requires the ports of different cells to *match* exactly in position and size.

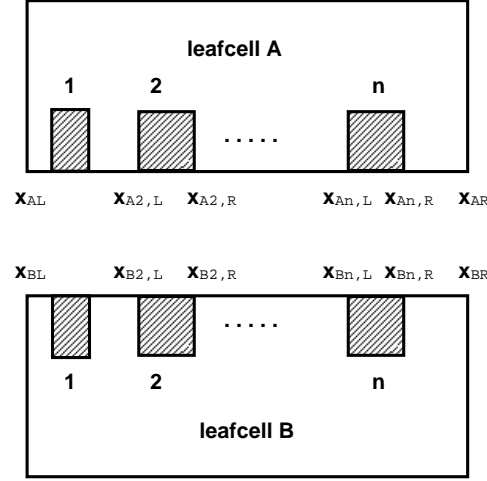


Figure 4.4: Port matching of leaf cells.

One naive way of translating the port matching constraints is to make the port spacings and port widths equal for all matching cells. The constraints result from Figure 4.4 are then:

$$x_{A,iL} - x_{A,(i-1)R} = x_{B,iL} - x_{B,(i-1)R} \quad (4.1)$$

$$x_{A,iR} - x_{A,iL} = x_{B,iR} - x_{B,iL} \quad (4.2)$$

and relative port positions on the cell boundary are also set to equal:

$$x_{A,1L} - x_{AL} = x_{B,1L} - x_{BL} \quad (4.3)$$

$$x_{AR} - x_{A,nR} = x_{BR} - x_{B,nR} \quad (4.4)$$

The problem of this approach is that the constraints bind variables from different cells together. Therefore they have to be migrated simultaneously. This may increase the number of variables in the underlying ILP solver substantially. With large datapath library, this approach quickly becomes infeasible.

We instead introduce a pair of constants, d and w to break the dependency between different cells:

$$x_{A,iL} - x_{A,(i-1)R} = d \quad x_{B,iL} - x_{B,(i-1)R} = d \quad (4.5)$$

$$x_{A,iR} - x_{A,iL} = w \quad x_{B,iR} - x_{B,iL} = w \quad (4.6)$$

Because d and w are constants, with constraints in Equation 4.5 and 4.6 leaf cells can still be migrated separately. However, the value of d and w must be carefully selected so that constraints in Equation 4.5 and 4.6 do not conflict with design rule constraints described in Chapter 3. To address this problem, we employ a dual-pass strategy that is elaborated below:

- In the first pass, it analyzes the layout of each leaf cell, generates the design rule constraints, and drives an ILP solver under the objective function that the designer needs to arrive at a temporary migration solution of each cell as shown in Figure 4.5. Note that the ILP problems are solved separately for different cells.
- In the second pass, the different architectural and circuit requirements are translated into linear constraints, such as the port matching constraints in Equation 4.5. Here, the temporary solution obtained in the first pass is exploited so that the new constraints relate variables originating from the same cell. The ILP solver is then called again to obtain the new and final solution to accommodate the new constraints. Note again that the ILP problems are solved separately for each cell.

Using this dual-pass strategy, We obtain d and w by taking the maximum value of $x'_{iL} - x'_{(i-1)R}$, and $x'_{iR} - x'_{iL}$ among all the leaf cells that have to be matched, where x' is the temporary solution we obtain in the first pass. This method effectively stretches the port whose width or spacing to the previous port can be smaller than the maximum value among all the leaf cells, making all ports align together without design rule violations.

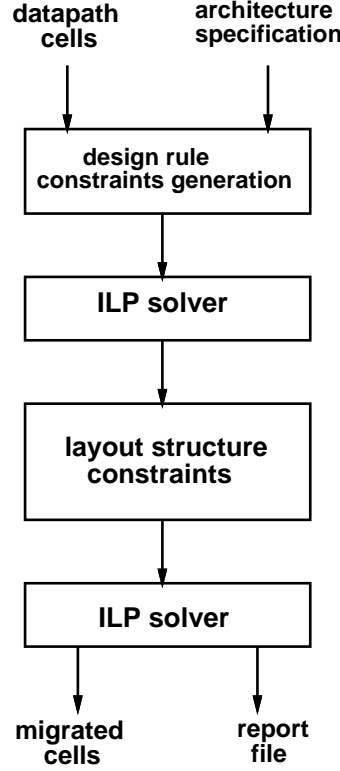


Figure 4.5: Dual-pass migration strategy.

4.1.2 Routing Track Matching

Data signals in the datapath are always routed horizontally (perpendicular to control signals), and over-the-cell, as the feedthroughs in our datapath leaf cells shown in Figure 4.3. Typically, they have to be aligned to a routing grid, for which the new migrated library may be different than the original. For example, for a leaf cell layout given in Figure 4.6, and a routing grid characterized by $\langle rs, ro, rw \rangle$, representing the routing pitch, offset and width respectively. The value of rs , ro and rw is specified by the designer in the architecture specification file in Figure 4.5. The Y coordinate of the bottom and top edge of each feedthrough, y_{iB} and y_{iT} in Figure 4.6, must satisfy constraints:

$$y_{(i-1)B} - K \cdot rs = y_{iT} \quad (4.7)$$

$$K \geq 0 \quad (4.8)$$

$$y_{iT} - y_{iB} = rw \quad (4.9)$$

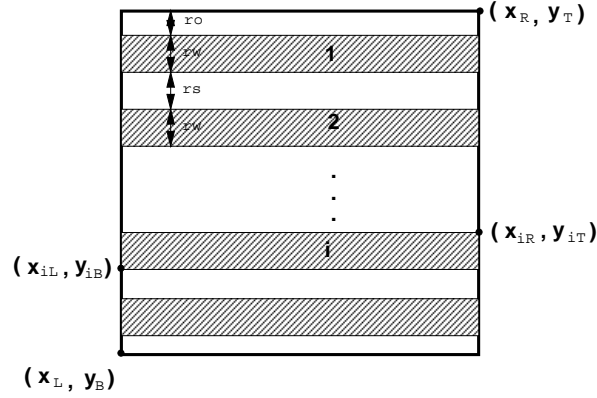


Figure 4.6: Cell with routing track for data signals.

while the Y coordinate of the top edge of the first feedthrough must satisfy constraints:

$$y_T - ro = y_{iT} \quad (4.10)$$

As the feedthrough covers the entire layout in the X direction, the left edge and right edge of each feedthrough must align the left boundary and right boundary of the leaf cell, which can be translated into constraints:

$$x_{iL} = x_L \quad (4.11)$$

$$x_{iR} = x_R \quad (4.12)$$

4.1.3 Power/Ground Net Sizing and Transistor Sizing

There are two kinds of constraints involved with power/ground nets. First, power/ground ports of abutting cells have to match. This can be solved by the port matching method described

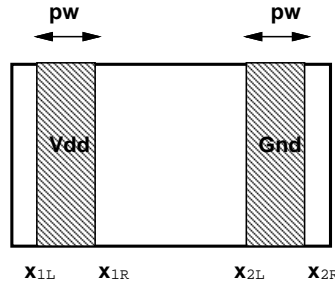


Figure 4.7: The width of each power net has to be equal to pw given by the designer in the specification file.

earlier. Second, the width of the power/ground net needs to satisfy the architectural specification as shown in Figure 4.7. Often, the width is determined by separate power/ground design methodology and layout migration has to faithfully follow the specification. These constraints are expressed as follows:

$$x_{iR} - x_{iL} = pw \quad (4.13)$$

where x_{iL} and x_{iR} are the left edge and right edge of the power/ground net respectively and pw is the user specified width of the power line.

Similarly, a circuit-level transistor sizing tool may determine an optimal transistor size that is different from the original layout, and it will rely on the migration tool to perform the change. After the identification of transistors in the layout, the sizing requirement can be expressed as an equality constraint, i.e the width and length of each transistor are set to the value as specified. Note that we only expect modest change in the transistor size, and therefore mild change in layout topology. For example, the introduction or elimination of transistor fingers is not needed.

4.1.4 Soft Constraints

A practical problem frequently encountered is that it is highly possible that the layout architecture specified by the user may lead to infeasible solutions. For example, if the routing pitch rs and routing width rw are too small, the routing grid constraints may conflict with minimum spacing requirement and minimum width requirement on metal2 specified by design rules in the new technology file. The ILP solver only provides a binary answer of failure when the given constraints are conflicting with each other. To make things worse, a typical leaf cell may have over thousands of constraints. It is unlikely that the user can trace where the conflicting constraints are and make a decision on where to change architecture specification or manually modify the layout at some specific location. It is instead highly desirable for the tool to provide some hints.

We introduce a new concept, called *soft constraints* to address this problem. Typically, the constraints that are related to architecture specification given by the designer, such as routing track constraints, power/ground sizing constraints, and transistor sizing constraints, will be introduced as soft constraints, in contrast to hard constraints such as design rule constraints. One of the characteristics of these constraints is that they are all expressed as equalities. Consider such equality constraints expressed in the form of:

$$\sum_j A_{ij}x_j = b_i \quad (4.14)$$

Where A_{ij} is the coefficient matrix, and b_i is a vector of constraints. We introduce two positive variables, called *elastic variables* e_{i1} and e_{i2} that will be added to the equality:

$$\sum_j A_{ij}x_j + e_{i1} - e_{i2} \geq b_i \quad (4.15)$$

$$e_{i1} \geq 0 \quad (4.16)$$

$$e_{i2} \geq 0 \quad (4.17)$$

Since the values of $e_{i1} - e_{i2}$ can be set arbitrarily in value, the original constraint can be relaxed or *softened*, in other words, the equalities do not have to be satisfied. This effectively enlarges the feasible solution space of the ILP problem.

On the other hand, it is highly possible that the soft variables may make those constraints that can be satisfied become infeasible by setting the soft variables to a non-zero value. To prevent unnecessary constraints relaxation, we penalize those solutions that were not supposed to be feasible originally by adding them to the objective function with a large weighting factor. Combining Equation (3.5), the new objective function becomes

$$\sum_j (R_j - L_j) + W \sum_i (e_{i1} + e_{i2}) \quad (4.18)$$

This way, if conflicting constraints exist, by looking for all non-zero elastic variables, users can easily pinpoint the wrong specifications and revise them accordingly.

4.2 Standard Cell Library Migration

Standard cell library is the basic library used for most ASIC designs. It provides functional blocks such as inverters, NANDs, and flip-flops used for synthesis and layout presentation of these function blocks for place & route. An example of design implemented with standard cell library that consists of rows of standard cells and channels between them is given in Figure 4.8 [14]. More advanced design with more than two layers for routing may not leave the space for channels which means that routings are all done over the cell.

There are several factors that impact the design of standard cell libraries. First, with the modern synthesis design flow, circuit designers usually do not see the layout cells. So there is great need for standardization of leaf cells in the library. The standardization includes the requirements such as [7]:

- The shape of leaf cells must be rectangle.
- Cells in the same row or in particular are all of the same height.

- Power lines should have the same width and same position for all the cells in the library.

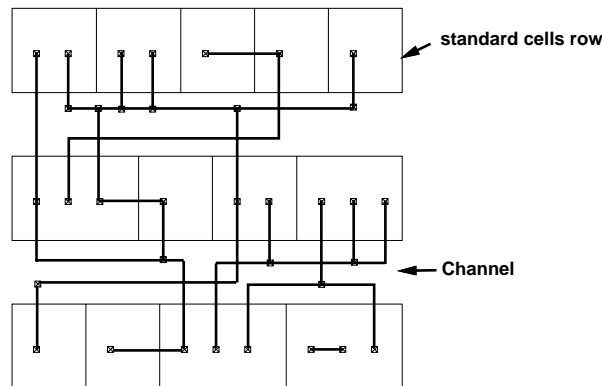


Figure 4.8: Standard cells design

Another factor that impacts standard cells design is the influence of place and route tools. The connectivity between cells at the same row or in different row is done by the router which only works well with cells designed in a certain pattern. Cells design is highly influenced by the restriction of these tools. Some of the considerations related with routing are listed here:

- All the input and output ports must have a predefined layer, position, shape and size. These characteristics are decided with considerations of requirements from place & route tool.
- The cell width must be rounded up to multiple of coarse grid. The grid size is determined by the desire to make placement easier.
- The placement of N transistors, P transistors, poly and wells should carefully follow the same guidelines so that no design rule violations are created when cells are abutted.

4.2.1 Layout Structure Constraints Generation for Standard Cells

Figure 4.9 shows a summary of layout structure requirements for standard cell library developed by Tim Burd from University of California, Berkeley [3]. We will use this design as an example to illustrate the architecture constraint generation process.

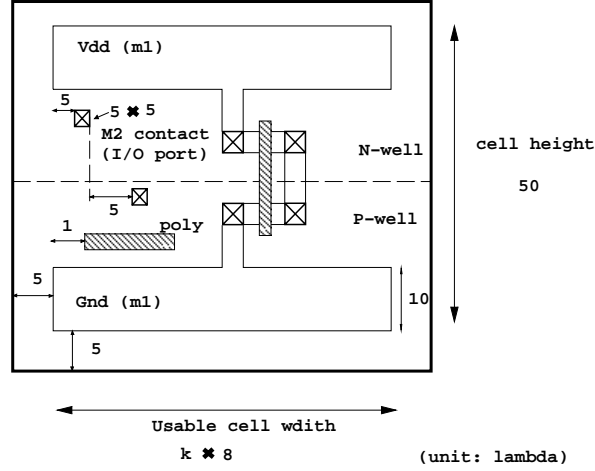


Figure 4.9: Layout architecture for a standard cell library.

- An I/O port is defined by a labeled metal2 contact, the shape of which is a $CW \times CW$ square (CW is equal to 5λ in Figure 4.9). As the placement and routing tool for this library uses fixed-grid two-level routing, it requires that all I/O ports stay in fixed grids as shown in Figure 4.10. Each port has CS spacing along the horizontal axis, with an offset of CO from either side of the power rail (CS and CO are set to 5λ and 5λ in Figure 4.9). Let x_{iL} and x_{iR} denote the X coordinates of each port's left edge and right edge, y_{iB} and y_{iT} denote the Y coordinates of each port's bottom edge and top edge. The grid requirements for I/O ports are translated into constraints below:

$$x_{iR} - x_{iL} + ex_{i1} - ex_{i2} = CW \quad ex_{i1} \geq 0 \quad ex_{i2} \geq 0 \quad (4.19)$$

$$y_{iT} - y_{iB} + ey_{i1} - ey_{i2} = CW \quad ey_{i1} \geq 0 \quad ey_{i2} \geq 0 \quad (4.20)$$

$$x_{iL} - x_{(i-1)R} + es_{i1} - es_{i2} = k_i \cdot (CW + CS) + CW \quad (4.21)$$

$$k_i \geq 0 \quad es_{i1} \geq 0 \quad es_{i2} \geq 0 \quad (4.22)$$

Where ex_{i1} , ex_{i2} , ey_{i1} , ey_{i2} , es_{i1} and es_{i2} are elastic variables used to trace conflicting constraints when the constants given by the designer cause design rule violations as discussed in Section 4.1.4. Since in real design, it is not necessary to have all the ports

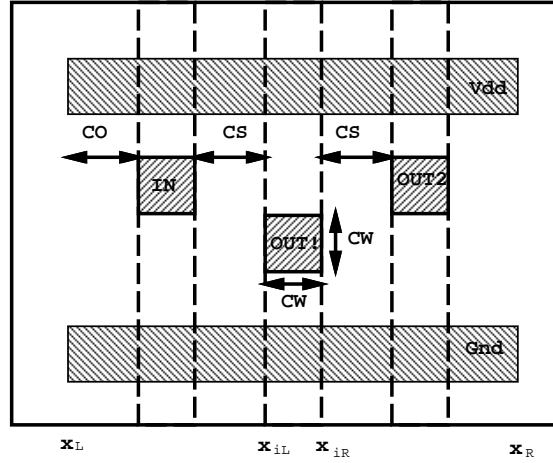


Figure 4.10: All I/O ports stay in fixed grids

in every other grid, the spacing of the ports is set to $k_i \cdot (CW + CS) + CW$ instead of CW in Equation 4.21.

- The placement & route tool require that each cell in the library has identical usable cell height H that is 50λ in Figure 4.9 and the overall width of the cell is a multiple of a constant W which equals to 8λ in Figure 4.9. Given cell topology in Figure 4.11, the cell width and height requirement can be translated into equality constraints:

$$y_{dT} - y_{gB} + e_{H1} - e_{H2} = H \quad (4.23)$$

$$e_{H1} \geq 0 \quad e_{H2} \geq 0 \quad (4.24)$$

$$x_{dR} - x_{dL} + e_{W1} - e_{W2} = W \quad (4.25)$$

$$e_{W1} \geq 0 \quad e_{W2} \geq 0 \quad (4.26)$$

- The width of power rails is set to a value defined by circuit designer with considerations that the power supply connections will meet electromigration requirements and resistance characteristics. In our migration tool, this requirement can be modeled as setting power rail width to a constant value PW . Take Vdd rail in Figure 4.11 as an example,

the width constraint is translated as:

$$y_{dT} - y_{dB} + e_{P1} - e_{P2} = PW \quad (4.27)$$

$$e_{P1} \geq 0 \quad e_{P2} \geq 0 \quad (4.28)$$

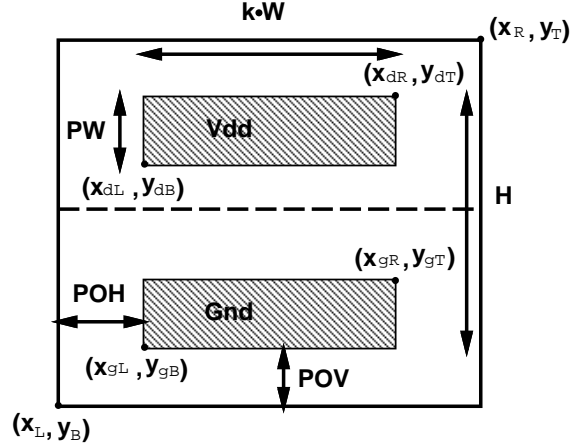


Figure 4.11: The requirements on power rails

- There is certain well overlap denoted as POV in Figure 4.11 (POV is equal to 5λ in Figure 4.9) along the vertical axis to guarantee that the active tiles can be placed all the way to the outer edge of power rails without violating the overlap rule between active and well. Although design rule constraints generation can guarantee that the overlap is large enough, different cell may turn out with different overlap after migration, which makes power rails not aligned when different cells are abutted. So, we set the overlap between power rail and well all the same:

$$y_{gT} - y_{gB} + e_{OV1} - e_{OV2} = PW \quad (4.29)$$

$$e_{OV1} \geq 0 \quad e_{OV2} \geq 0 \quad (4.30)$$

There is also POH well overlap along the horizontal axis. The constraint for horizontal overlap can be generated in the same way as the vertical overlap constraint. As the cells are

abutted along horizontal axis, all active, metal1 and metal2 tiles must be contained within two power rails. This is guaranteed by the original careful design because migration will not make drastic topology changes which means that the tiles inside power rails will not move outside after migration.

Chapter 5

Experiments and Conclusion

5.1 Experimental Setup

We implemented the migration tool on top of an IP-centric CAD infrastructure, called *ipsuite*, which uses Magic’s corner stitching data structure to represent mask layout. An open-source ILP solver *lp_solve*, by Michel Berkelaar from Northwestern University and Argonne National Laboratory, is used to generate the optimized result. For all the test libraries, including the datapath library and the standard cell library, there will be up to 2,000 variables and 40,000 constraints (shown in Appendix A and B). The ILP solver can solve the ILP problem with as many as 30,000 variables and 50,000 constraints, which fits our requirement. The migration tool itself is implemented by over 12,000 lines of C code.

To test the effectiveness of our tool, we apply our tool on the low-power standard library and datapath library developed by Burd [3] at University of California, Berkeley. Standard cell library contains 94 leaf cells that include the range of 2, 3 and 4 input “simple” gates – nand/and, nor/or, muxes, and-or/or-and, etc. There are various-sized inverters, buffers, transmission gates and a small variety of simple latches. Different types of adder and subtractor bit slices are also included in the standard cell library. The datapath library contains 285 cells that have a wide variety of functions as those in standard cell library. Several chips such as protocol

chip, video decompression chip set are designed with these libraries [3]. Both standard cell library and datapath library are implemented based on standard MOSIS $1.2\mu m$ process. Our targeted process is TSMC $0.25\mu m$ and TSMC $0.18\mu m$ technologies.

In the following sections, we show the experimental results to demonstrate each feature of our migration tool. Section 5.2.1 gives the run time result for constraint generation algorithm and ILP solver. The run time for constraint generation is found to be propotional to $O(N^{1.4})$. In order to demonstrate that *Dual-pass strategy* is effective in solving hierachical layout migration problems, such as pitch matching problem, we give the experimental results of migrating leaf-cells for a N bit adder in datapath library, and migrating two datapath library cells *andf201* and *muxf201* with respect to layout architecture requirements in section 5.2.2. The *soft constraints* method is tested in section 5.2.4 with an example migration result of a standard cell. And the soft constraint method is found to be effective in correcting wrong constraints and guiding the users to fix them. Finally, a comparision of different objective functions is presented in section 5.2.3 with migration result of a standard cell under different objective functions.

5.2 Experimental Result

5.2.1 Run Time

The run time of datapath library and standard cell library is summarized in Appendix . Figure 5.1 gives a plot of run time versus number of tiles in the layout. The solid line in the figure shows the run time (measured in seconds) of constraints generation for standard cells versus the number of tiles N . And the dotted line is the plot of function proportional to $f(N) = N^{1.4}$.

The run time in Figure 5.1 includes *IntraPlane*, *InterPlane*, *InterPass* and *Connect* constraint generation. Except from *Connect* constraint generation, other constraint generation algorithms are all based on *Depth-K searching* algorithm. Because most layouts have very few contacts, we can assume that this run time is dominated by the run time of constraint generation using *Depth-K searching* algorithm. As can be seen from Figure 5.1, this real run

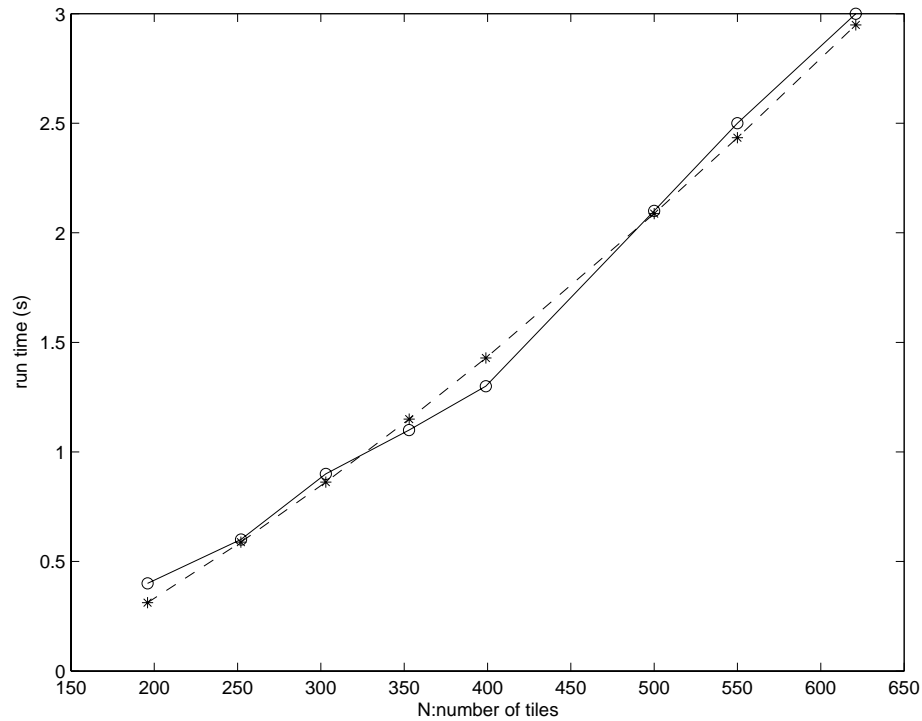


Figure 5.1: The run time of design rule constraint generation

time curve fits the function $f(N)$ very well and this gives the result: the expected running time for constraint generation with *Depth-K searching* algorithm is $O(N^{1.4})$ within the range where $N \in [0 : 700]$.

Figure 5.2 shows the run time of ILP versus number of tiles. As we can observe, the run time of ILP dominates the whole computation time. The ILP problem is known to be an NP-hard. The simplex algorithm, which is the basis of ILP solver, is found to be exponential in the number of decision variables [23]. However, as the complexity of each leafcell is limited, total migration time is limited in minutes and thus still tolerable.

5.2.2 Dual-pass strategy

The *dual-pass strategy* is used to accommodate layout architecture constraints with design rule constraints that have been built. In this section, we give the migration result for the ripple carry

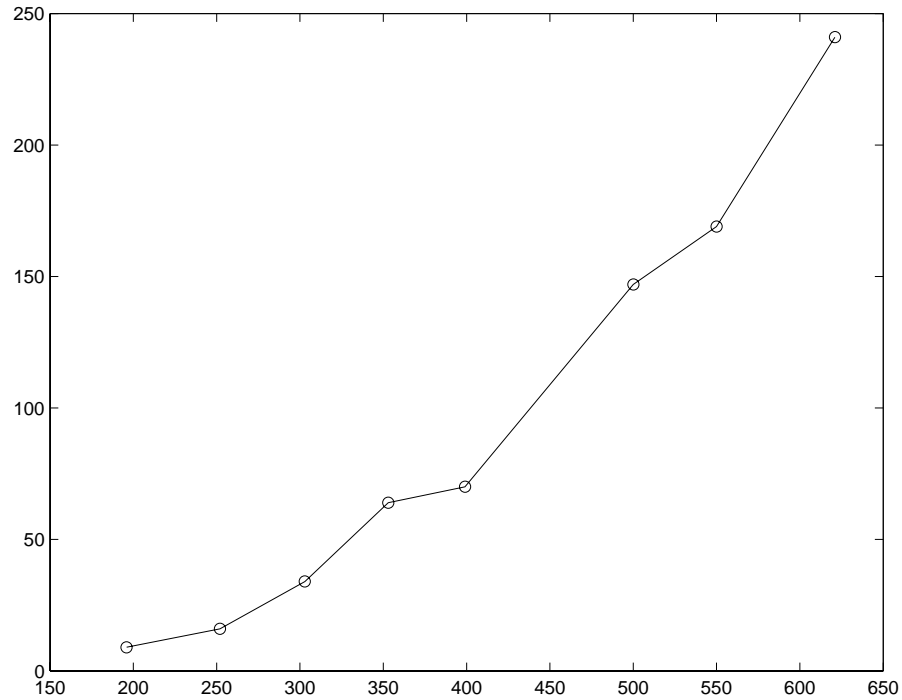


Figure 5.2: The run time of ILP solver.

adder in datapath library and two leafcells in standard cell library to demonstrate the result for this algorithm.

In this datapath library, there are four leafcells used for building a ripple carry adder. Cell *add* and cell *add_fast* are full adder bit slices. Cell *add_cs_sel* and *add_cs_0* are control slices used to determine the carry-in signal for the least significant bit adder cell. Figure 5.3 shows the leafcells before migration and after migration. The old layouts are based on standard MOSIS $1.2\mu m$ technology, and the news cells are generated after the migration process under the geometric closeness objective function. The targeted process is TSMC $0.25\mu m$ technology. Note that the layouts are displayed with measurement unit set to 2λ .

The usage of these cells for building an N bit adder are visualized in Figure 5.4.

The layout architecture characteristics before migration and after migration are summarized in Table 5.1.

Figure 5.5(a) and (b) shows a four-bit adder built from old leafcells and from migrated

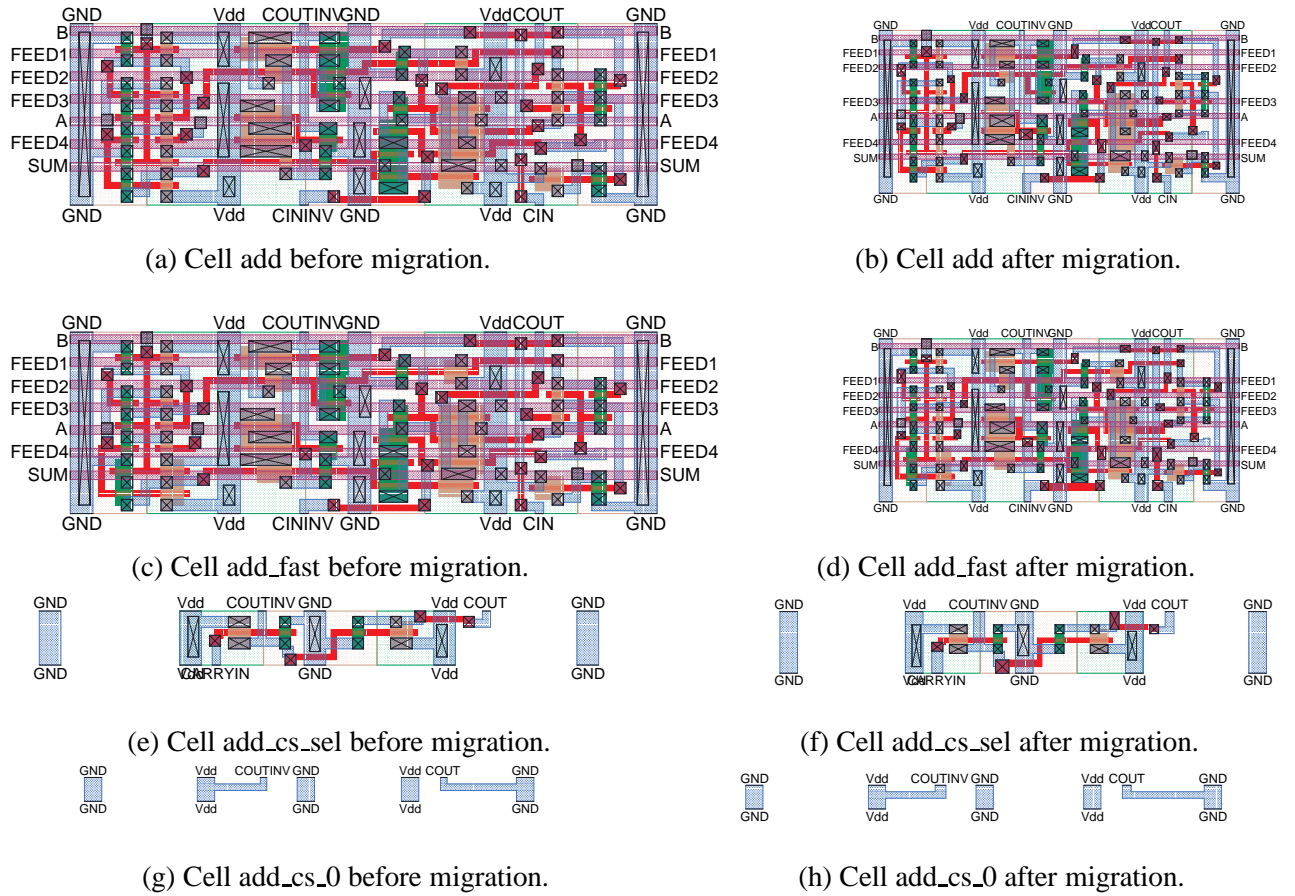


Figure 5.3: The leafcells for ripple carry adder

Table 5.1: Layout architecture characteristics

Height of bit slice (old/new)	Width of power rails (old/new)	Feedthrough (old/new)		
		width	spacing	offset
$64\lambda/100\lambda$	$8\lambda/8\lambda$	$3\lambda/3\lambda$	$5\lambda/6\lambda$	$1\lambda/3\lambda$

leafcells respectively. Both adders are scaled to the same width for comparison. The result shows that:

- All the ports such as *CARRYIN*, *CARRYOUT*, *Vdd* and *GND* are correctly matched both in position and in size between abutting cells.

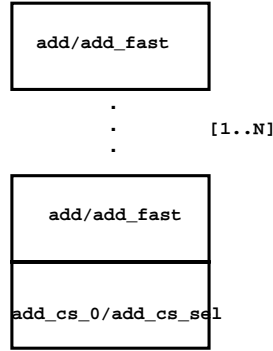


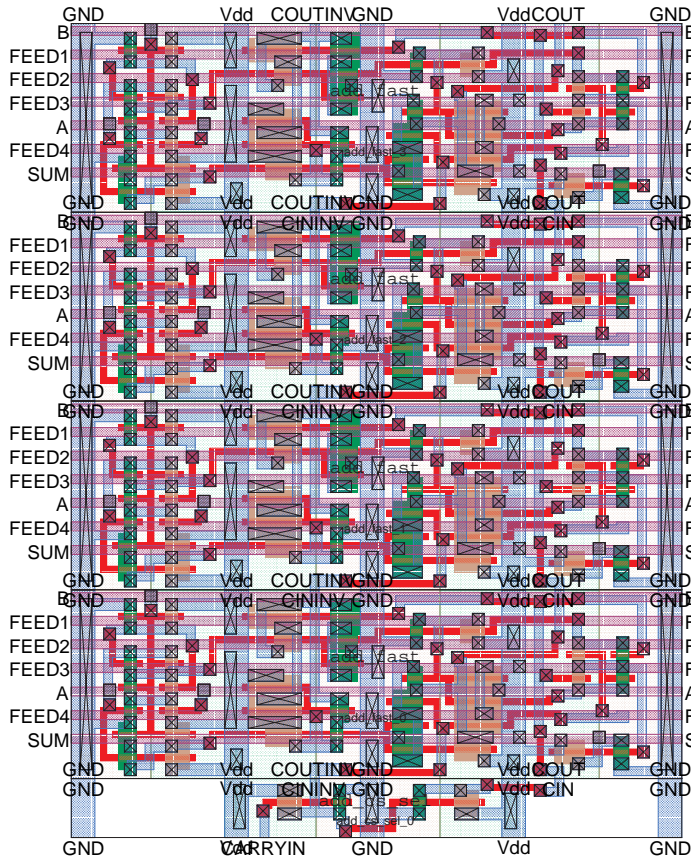
Figure 5.4: The floorplane of an N bit adder.

- The feedthroughs are placed in grid according to the requirements given in Table 5.1.
- Other requirements such as cell height and power rail requirements are all met.

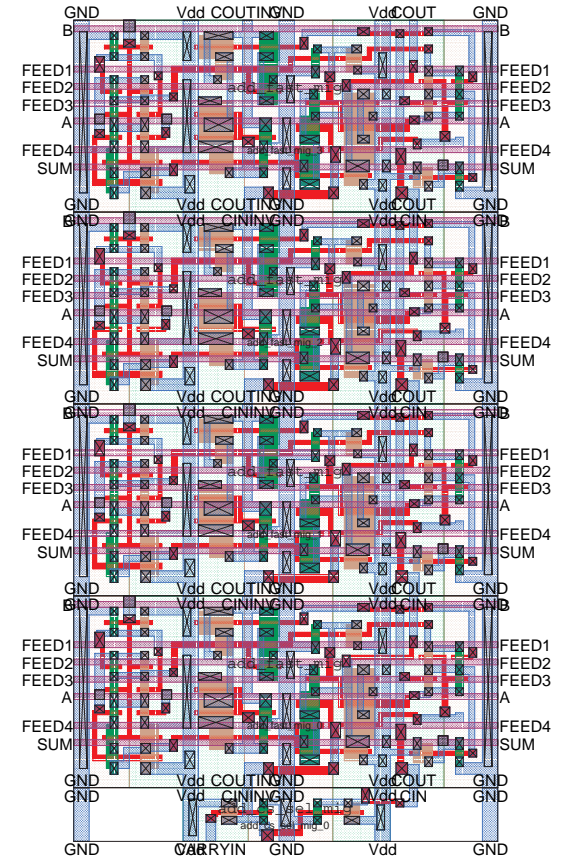
Figure 5.6 shows two example leafcells *andf201* and *muxf201* based on standard MOSIS $1.2\mu m$ technology in standard cell library and Figure 5.7 gives the migration result. The layout structure requirements are given in Table 5.2. The migrated cells satisfy all the requirements listed.

5.2.3 Geometric Closeness Objective Function

As discussed in Chapter 3, the geometric closeness objective function is adopted to keep the original shape of the layout to a maximum extend. Figure 5.8 shows an example to compare the migration result under geometric closeness objective function and minimum perturbation objective function. Note that the height of the substrated contact in *GND* rail in Figure 5.8(a) is kept the same as in Figure 5.8(c), while the height in Figure 5.8(b) is larger than the old layout. This is due to the fact that when overlap between power rail and well is reduced by 1λ , the minimum perturbation objective function makes the contact snapped to the original position and its height is thus increased by 1λ . Although this may not be a big improvement for this specific digital circuit, we would expect that the geometric closeness objective function plays a more important role for less aggressively circuits and analog circuits.



(a) A four-bit adder based
on MOSIS 1.2 μ m technology



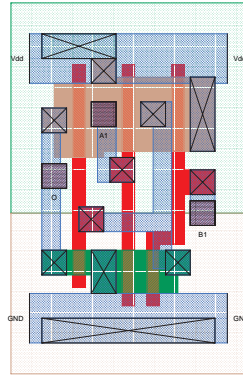
(b) The adder with migrated leafcells
based on TSMC 0.25 μ m technology

Figure 5.5: Migration of a four-bit adder

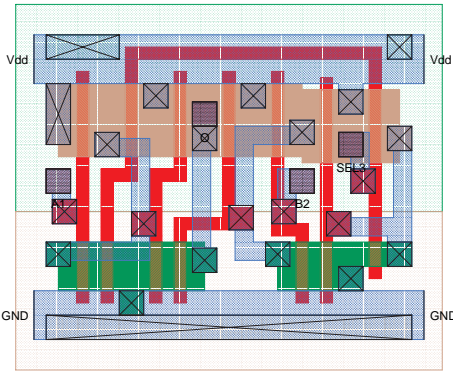
5.2.4 Soft Constraints

Soft constraints method is employed to trace the conflicting constraints when the layout architecture requirements set by user are contradictory to design rule constraints. The migration result for cell haf001 shown in Figure 5.9 and 5.10 gives a demonstration of the benefit from this method.

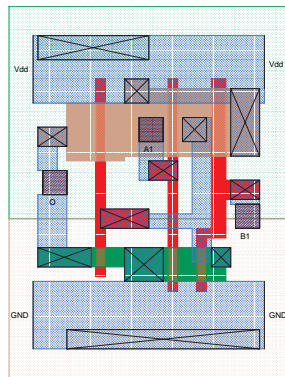
The user specified layout architecture requirements are given in Table 5.3. Note that there are two requirements in this table that conflict with design rules. First, the minimum size rule for metal2 contact is 5λ according to design rule (Mosis #8.1) in TSMC 0.18 μ m technology. However, port size is specified to be $4\lambda \times 4\lambda$, which violates the rule. The second unreasonable



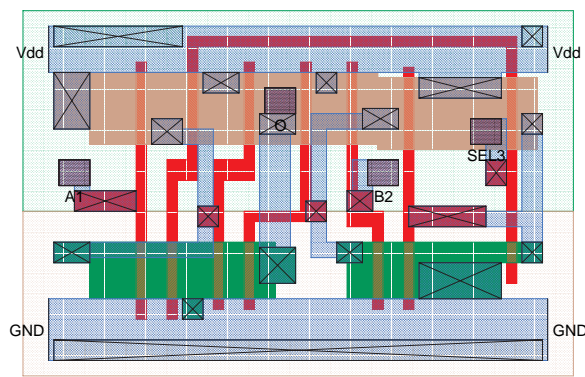
(a) Cell andf201



(b) Cell muxf201

Figure 5.6: Two old standard cells based on standard MOSIS $1.2\mu m$ technology.

(a) Cell andf201



(b) Cell muxf201

Figure 5.7: Migrated cells based on TSMC $0.18\mu m$ technology.

requirement is the power width requirement. According to design rule Mosis #6.1 and #6B.4,5, the minimum width of diffusion contact must be greater than 4λ and the minimum spacing between diffusion contact must be greater than 4λ . So the minimum power rail width must be greater than 12λ as shown in Figure 5.11, which is contradictory to user specified value 8λ .

Instead of simply giving the user a binary answer such as “This is an infeasible solution”, soft constraints method generates a design rule clean layout that discards the conflicting user specified constraints. The migrated layout has port size set to 5λ and GND line width set to 12λ . A report about the wrong constraints is also given to help the user correct the wrong

Table 5.2: Layout structure characteristics

Old cells	usable cell height		50λ
	usable cell width		$k \cdot 8\lambda$
	power	width	8λ
		vertical overlap between well	5λ
	rails	horizontal overlap between well	3λ
		size	$4\lambda \times 4\lambda$
	port	spacing	$k \cdot 4\lambda$
		offset	2λ
Migrated cells	usable cell height		65λ
	usable cell width		$k \cdot 8\lambda$
	power	width	14λ
		vertical overlap between well	6λ
	rails	horizontal overlap between well	5λ
		size	$5\lambda \times 5\lambda$
	port	spacing	$k \cdot 5\lambda$
		offset	2λ

specifications:

Error message

Port size is increased by 1λ .

Power rail width is increased by 4λ .

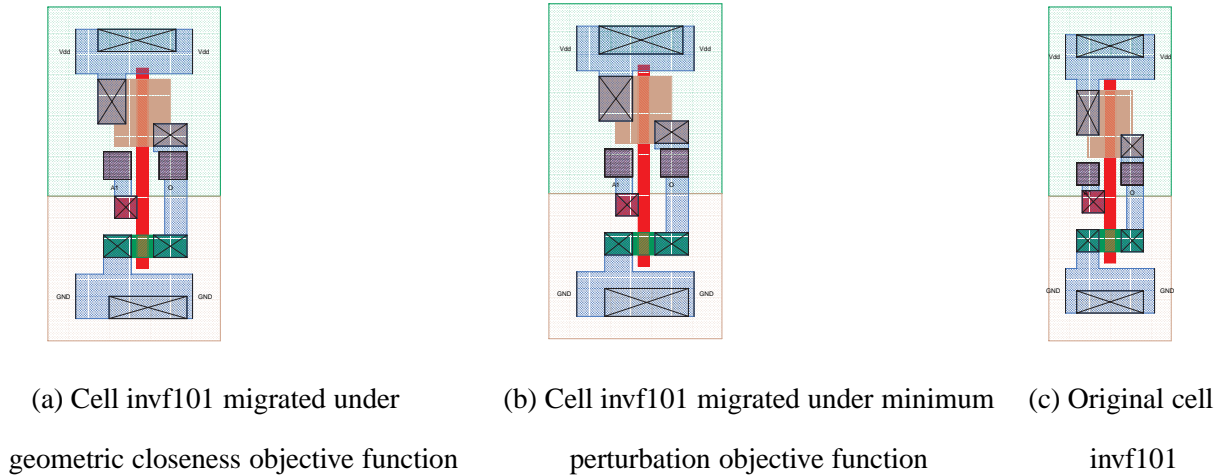


Figure 5.8: The migration results under geometric closeness objective function and minimum perturbation objective function.

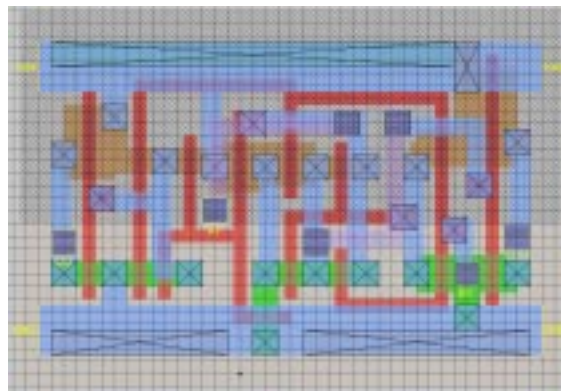


Figure 5.9: Cell haf001 before migration

5.3 Limiation

Some limitations of our tool that can be observed from the experimental results are listed below:

- As we can see from Figure 5.7(b), three contacts are greatly stretched in the X direction after migration. This is due to the InterPass constraints that require the relative position of edges keep unchanged. The right edges of these contacts stretched are all on the right side of port *SEL* in the original layout. After migration, the spacing requirements of ports make *SEL* moving rightward, which make other contacts stretched at the same time.



Figure 5.10: Cell haf001 after migrated towards TSMC $0.18\mu m$ technology.

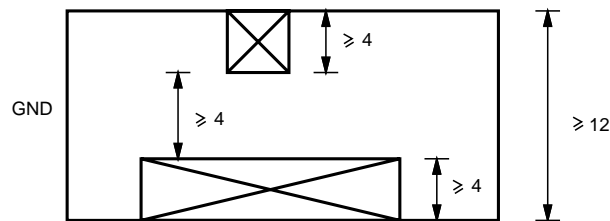


Figure 5.11: The design rule requirements on power rail.

Although the contact stretching may not make a big difference in circuit performance, this mechanism has potential to stretch some important tiles such as transistors, which will affect the circuit performance. In other words, the tool needs some “intelligence” to analyze that in which situation the layout is over-constrained by InterPass constraints. One of the methods to solve this problem is by adopting two-dimensional compaction method, which can take care of X-compaction and Y-compaction at the same time.

- There is still no effective way to do transistor sizing. And the shape of transistors are fixed to the original one. The tool still cannot allow the insertion of transistor fingers.

Table 5.3: User specified layout architecture requirements for cell haf001

usable cell height	65λ	
usable cell width	$k \cdot 8\lambda$	
power rails	width	8λ
	vertical overlap between well	6λ
	horizontal overlap between well	5λ
port	size	$4\lambda \times 4\lambda$
	spacing	$k \cdot 5\lambda$
	offset	2λ

5.4 Conclusion

The quick update of technology and the complexity of SOC makes it necessary to develop a tool to migrate the old library leafcells to the new technology in order to save the library design cost for IP vendors. Traditionally, the migration tools are based on symbolic layout compaction techniques that were developed to compress the layout area and convert the symbolic layout to the actual mask layout. In this thesis, we demonstrate a layout migration engine can be applied directly to the actual mask layouts and migrate the layouts under the multiple choices of objectives such as minimum area, minimum perturbation or geometric closeness as discussed in Chapter 3. The fundamental algorithm for the migration engine is design constraint generation, which is used to perform the tedious tasks of determining geometric constraints between all edges. We develop a Depth-K searching algorithm, which limits the searching area within fixed number of depths for each design rule and thus saves checking time, to generate design rule constraints.

The migration tool also provides a comprehensive framework to handle the high level struc-

tural requirements on library leafcells so that after one migration, all library leafcells do not need to be migrated again with respect to specific circuits. By building soft constraints for high level structure requirements, the migration tool can give users a feedback when these requirements are not correctly set and guide users to the successful library migration.

We conducted our experiments on the standard cell library and datapath library developed by Burd at University of California, Berkeley. The experiments result show that the migrated layouts are design rule clean and respect the specified structural requirements.

5.5 Future work

There is a lot of space for future work for the migration tool. An important step would be performance characterization for the migrated layouts. Timing analysis needs to be carried out on new layouts for performance verification. More ambitious improvements such as transistor-sizing capability where layout topology can be changed to insert transistor fingers, as well as extending the application to other IP libraries can be included in the extension of our work.

Chapter 6

Appendix

The tables shown in the following give more comprehensive results carried out on a SUNBlade 100 system running at 500 MHZ. Here, related cells that need port matching are migrated in groups. The third column demonstrates two important figures, *ASR* is the actual area scaling ratio achieved, as measured by $\frac{\text{migrated layout area}}{\text{old layout area}}$, and *TSR* is the linear area scaling ratio measured by $(\frac{\text{migrated feature size}}{\text{old feature size}})^2$, which as we know, direct layout shrinking with this ratio may result in design rule violations. These two values are shown for both targeted technologies. The number of rectangles (including space) in the layout, and the total numbers of constraints generated are shown in the fourth and fifth column. The last two columns show the runtime spent on constraint generation (measured in seconds), and ILP solving (measured in minutes).

Original cell based on MOSIS 1.2 μ m technology	Migrated cell based on TSMC 0.25 μ m technology	Migrated cell based on TSMC 0.18 μ m technology
		
Cell aof2201		
		
Cell blf00101		
		
Cell buff101		
		
Cell buff121		

Table 6.1: Experiment results of datapath library migration.

Function unit	Cell name	ASR:TSR $0.25\mu\text{m} / 0.18\mu\text{m}$	Number of polygons	Number of constraints	constraints generation run time (s) $0.25\mu\text{m} / 0.18\mu\text{m}$	ILP solver run time (m) $0.25\mu\text{m} / 0.18\mu\text{m}$
adder	add	0.07:0.04 / 0.04:0.02	452	56127 / 36866	134.9 / 149.5	18.5 / 19
	add_cs_sel	0.06:0.04 / 0.03:0.02	71	4288 / 3070		
	add_cs_0	0.04:0.04 / 0.03:0.02	11	225 / 223		
subtractor	sub	0.07:0.04 / 0.04:0.02	479	36538 / 44535	136.7 / 114.4	20.6 / 19.8
	sub_cs_sel	0.06:0.04 / 0.03:0.02	72	3071 / 3071		
	sub_cs_1	0.03:0.04 / 0.015:0.02	11	229/229		
mux2	mux2	0.08:0.04 / 0.04:0.02	145	11797 / 7745	10.9 / 10.5	3.2 / 2.9
	mux2_cs1	0.06:0.04 / 0.03:0.02	52	4248 / 2203		
	mux2_cs2	0.06:0.04 / 0.027:0.02	61	4577 / 2279		
	mux2_cs3	0.07:0.04 / 0.03:0.02	104	7512 / 4771		
	mux2_cs4	0.06:0.04 / 0.027:0.02	149	11096 / 8518		
mux3	mux3	0.08:0.04 / 0.04:0.02	211	11768 / 11796	36.4/38.7	15.2 / 12.8
	mux3_cs1	0.06:0.04 / 0.03:0.02	247	14247 / 14243		
	mux3_cs2	0.06:0.04 / 0.03:0.02	248	14573 / 14574		
	mux3_cs3	0.07:0.04 / 0.03:0.02	293	17514 / 17512		
	mux3_cs4	0.06:0.04 / 0.03:0.02	331	21099 / 21098		
tribuf	tribuf1	0.07:0.04 / 0.03:0.02	151	7880 / 7880	7.8 / 8.1	1.1 / 1.7
	tribuf1_cs1	0.07:0.04 / 0.03:0.02	59	2641 / 2641		
	tribuf1_cs2	0.05:0.04 / 0.03:0.02	105	5856 / 4723		
	tribuf1_cs3	0.06:0.04 / 0.03:0.02	144	7164 / 7163		
register	rf0	0.06:0.04 / 0.03:0.02	66	2748 / 2748	3.7 / 3.9	0.6 / 0.6
	rf1	0.06:0.04 / 0.03:0.02	66	2756 / 2756		
	rf01_cs1	0.07:0.04 / 0.03:0.02	92	3516 / 3517		
	rf01_cs2	0.07:0.04 / 0.03:0.02	92	3584 / 3584		
	rf01_cs3	0.06:0.04 / 0.03:0.02	92	3464 / 3464		

Experiment results of datapath library (continued).

Function unit	Cell name	ASR:TSR $0.25\mu\text{m} / 0.18\mu\text{m}$	Number of polygons	Number of constraints	constraints generation run time (s) $0.25\mu\text{m} / 0.18\mu\text{m}$	ILP solver run time (m) $0.25\mu\text{m} / 0.18\mu\text{m}$
shifter	shcs1	0.06:0.04 / 0.03:0.02	87	3957 / 3957	8.9 / 8.7	0.8 / 0.8
	shl1bit	0.04:0.04 / 0.02:0.02	88	3921 / 3921		
	shl1end	0.05:0.04 / 0.02:0.02	81	3478 / 3478		
	shl1lsb	0.05:0.04 / 0.02:0.02	130	6539 / 6539		
inverter	invs	0.04:0.04 / 0.02:0.02	57	2029 / 2029	1.2 / 1.3	0.2 / 0.2
	invn	0.05:0.04 / 0.03:0.02	80	3098 / 3098		
random logic	and2blp	0.06:0.04 / 0.03:0.02	112	5940 / 5940	6.4 / 6.6	3.3 / 3.3
	nand2lp	0.05:0.04 / 0.03:0.02	83	4015 / 4015		
	nandand3lp	0.07:0.04 / 0.03:0.02	113	6706 / 6706		
	or2blp	0.06:0.04 / 0.03:0.02	99	5319 / 5319		
	xnor2lp	0.06:0.04 / 0.03:0.02	132	8075 / 8075		
	xor2lp	0.06:0.04 / 0.03:0.02	132	8003 / 8003		
pipeline tspr register	tspr	0.07:0.04 / 0.03:0.02	137	7580 / 7582	14.7 / 14.9	5.7 / 6.1
	tspr_fb	0.08:0.04 / 0.04:0.02	173	10637 / 10637		
	tspr_cs1	0.05:0.04 / 0.03:0.02	49	1792 / 1792		
	tspr_cs2	0.05:0.04 / 0.03:0.02	52	2003 / 2003		
	tspr_cs3	0.06:0.04 / 0.03:0.02	91	3792 / 3792		
	tspr_cs4	0.06:0.04 / 0.03:0.02	103	4602 / 4602		
	tspr_csi1	0.06:0.04 / 0.03:0.02	33	980 / 980		
	tspr_csi2	0.06:0.04 / 0.03:0.02	34	1110 / 1110		
	tspr_csi3	0.05:0.04 / 0.03:0.02	96	4595 / 4595		
	tspr_csi4	0.05:0.04 / 0.03:0.02	126	6008 / 6008		

Table 6.2: Experiment results for standard cell library migration.

Cell Name	Number of tiles	Number of constraints $0.25\mu m/0.18\mu m$	Constraint generation run time (s) $0.25\mu m/0.18\mu m$	ILP run time(s) $0.25\mu m/0.18\mu m$
andf201	187	4384/4378	0.3/0.3	8/14
andf301	243	6772/6264	0.6/0.6	16/27
andf401	286	7568/7578	0.7/0.8	27/40
aof2201	298	8562/8572	0.8/0.9	35/42
aof2301	410	12586/12620	1.2/1.3	73/80
aof3201	463	14930/14944	1.6/1.6	101/108
aof4201	550	18870/18888	2.5/2.5	169/199
aoif2201	241	6212/6222	0.6/0.6	18/19
blf00001	195	4233/4241	0.3/0.5	9/13
blf00101	193	4391/4379	0.5/0.5	11/15
buff101	140	2757/2761	0.3/0.3	3/6
buff102	169	3590/3594	0.3/0.3	5/8
buff103	188	4252/4257	0.3/0.4	8/10
buff104	191	4290/4294	0.4/0.4	9/11
buff105	220	5341/5345	0.5/0.5	11/18
buff106	222	5415/5419	0.5/0.5	12/19
buff121	252	6365/6371	0.6/0.6	16/25
buff122	273	7167/7173	0.6/0.6	21/36
buff123	378	11912/11918	1.2/1.6	57/95
buff124	372	12148/12154	1.2/1.4	59/74
buff125	406	13565/13571	1.5/1.6	68/83
buff126	399	13374/13380	1.3/1.6	70/83

Experiment results of standard cell library (continued 1).

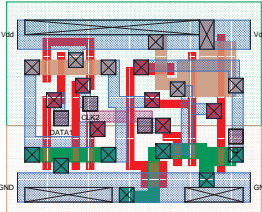
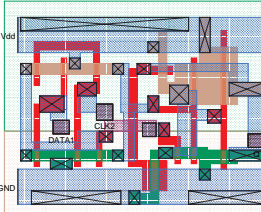
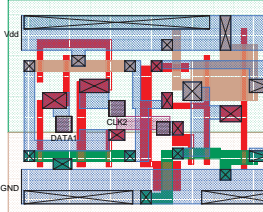
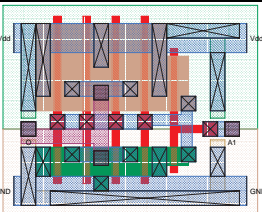
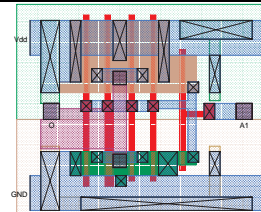
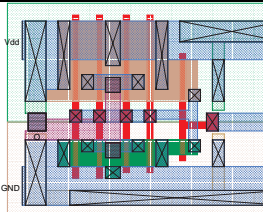
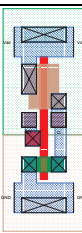
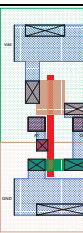
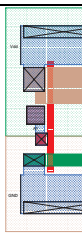
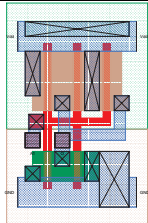
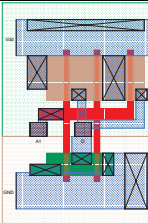
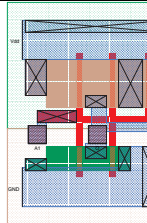
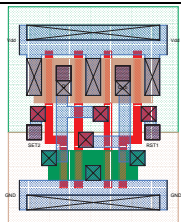
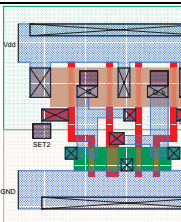
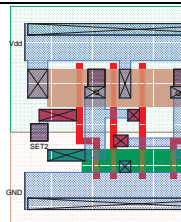
Cell Name	Number of tiles	Number of constraints $0.25\mu m/0.18\mu m$	Constraint generation run time (s) $0.25\mu m/0.18\mu m$	ILP run time(s) $0.25\mu m/0.18\mu m$
dfnf401	353	10705/10711	1.1/1.0	64/57
dfnf411	411	13245/13253	1.6/1.4	73/101
dfrf401	433	14133/14141	1.4/1.5	90/93
dfrf411	488	16615/16626	1.7/1.8	127/122
drif101	275	7692/7688	0.9/0.9	34/27
drif102	404	13109/13105	2.3/1.7	78/70
drif103	521	18054/18058	3.3/3.3	138/157
drif104	663	24415/24419	6.0/6.3	292/314
drif105	912	36074/36078	12.6/12.2	565/595
haf001	410	12861/12869	1.5/1.6	71/89
hsf001	421	13668/13676	1.5/1.3	74/79
invf101	100	1617/1621	0.2/0.2	1/2
invf102	127	2416/2420	0.3/0.2	3/3
invf103	128	2530/2534	0.2/0.3	3/4
invf104	144	2994/2998	0.3/0.4	5/6
invf121	196	4804/4810	0.4/0.6	9/10
invf201	155	3327/3335	0.4/0.4	5/6
invf202	154	3308/3325	0.3/0.3	6/7
labf111	213	5140/5148	0.5/0.5	12/13
labf211	237	5970/5962	0.6/0.6	15/14
lrbf202	76	1029/1033	0.1/0.1	1/2

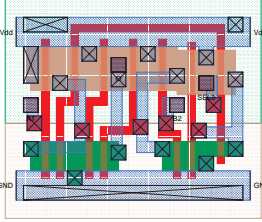
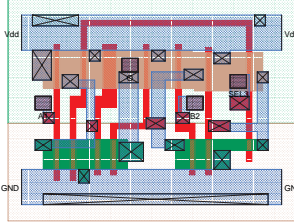
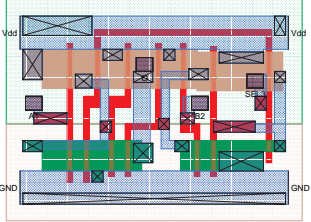
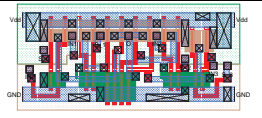
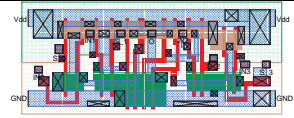
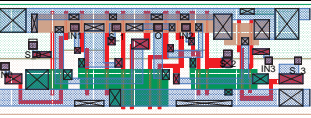
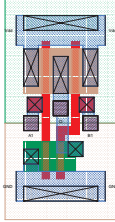
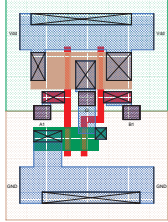
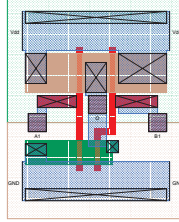
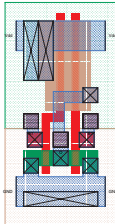
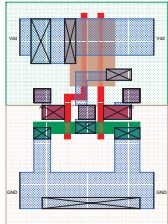
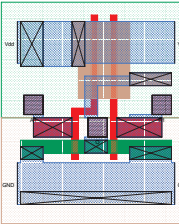
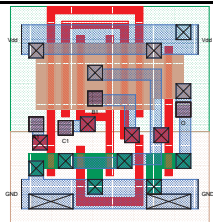
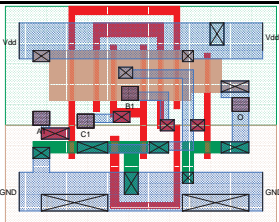
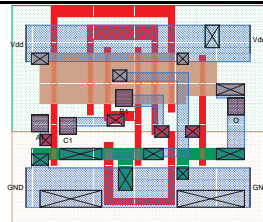
Experiment results of standard cell library (continued 2).

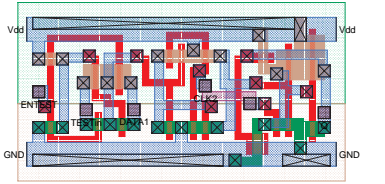
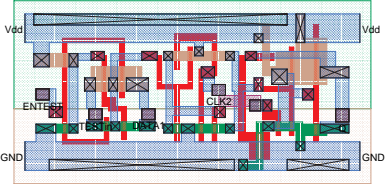
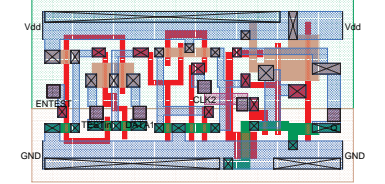
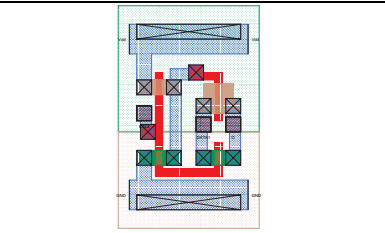
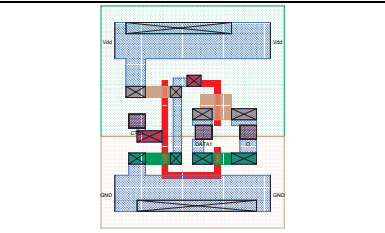
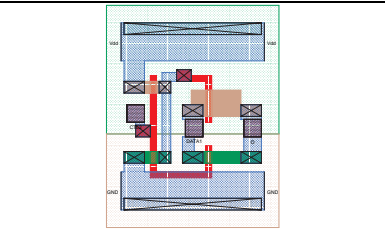
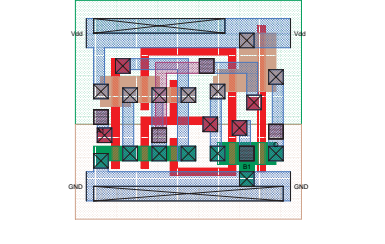
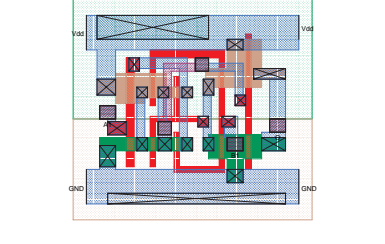
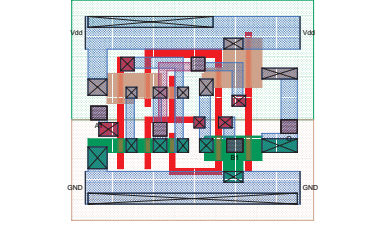
Cell Name	Number of tiles	Number of constraints $0.25\mu m/0.18\mu m$	Constraint generation run time (s) $0.25\mu m/0.18\mu m$	ILP run time(s) $0.25\mu m/0.18\mu m$
muxf201	337	10076/10080	1.1/1.1	42/44
muxf251	311	8828/8838	0.8/0.8	35/47
muxf301	639	23031/23043	3.0/2.9	233/308
muxf351	463	14930/14944	1.6/1.8	102/142
muxf401	993	40403/40417	6.7/6.4	704/822
muxf451	557	19340/19358	2.9/3.1	164/164
nanf201	143	2749/2755	0.3/0.3	4/4
nanf202	138	2640/2634	0.2/0.3	4/3
nanf211	197	4686/4694	0.4/0.4	11/10
nanf251	181	4094/4100	0.4/0.4	8/11
nanf301	179	3728/3736	0.4/0.4	6/12
nanf311	249	6420/6430	0.6/0.5	17/29
nanf401	240	5588/5598	0.6/0.5	16/21
nanf411	297	7893/7905	0.7/0.7	31/34
norf201	141	2684/2690	0.3/0.4	4/4
norf211	202	4749/4757	0.5/0.5	12/11
norf251	209	5354/5360	0.6/0.5	14/12
norf301	229	6074/6082	0.5/0.6	16/18
norf311	280	7465/7475	0.6/0.7	32/36
norf401	275	7773/7386	0.8/0.8	29/29
norf411	344	10168/10180	1.1/0.9	58/75

Experiment results of standard cell library (continued 3).

Cell Name	Number of tiles	Number of constraints $0.25\mu m/0.18\mu m$	Constraint generation run time (s) $0.25\mu m/0.18\mu m$	ILP run time(s) $0.25\mu m/0.18\mu m$
oaif2201	243	6009/6019	0.5/0.6	20/17
orf201	189	4401/4407	0.5/0.6	10/10
orf301	272	7254/7262	0.8/0.9	26/31
orf401	338	10019/10029	1.1/1.0	52/44
pudf000	52	517/519	0.1/0.1	1/1
puuf000	52	527/529	0.1/0.1	1/1
sdnf401	499	17111/17121	2.1/1.9	147/168
sdnf411	557	19845/19875	2.5/2.7	211/210
sdrf401	563	19723/19735	2.8/2.6	202/213
sdrf411	621	22387/22401	3.0/3.1	241/239
swcf020	154	3225/3219	0.3/0.4	6/4
swcf022	170	3965/3971	0.5/0.4	8/7
swcf023	168	3793/3799	0.4/0.4	9/8
swcf024	191	4709/4702	0.4/0.5	16/10
swcf120	160	3343/3337	0.4/0.4	7/6
swcf122	175	4070/4064	0.4/0.4	9/7
swcf123	172	3904/3898	0.4/0.4	10/7
swcf124	189	4606/4600	0.5/0.4	11/10
xnof201	307	8924/8930	0.8/0.8	37/36
xorf201	303	8716/8722	0.9/0.7	34/45

Original cell based on MOSIS 1.2 μ m technology	Migrated cell based on TSMC 0.25 μ m technology	Migrated cell based on TSMC 0.18 μ m technology
		
Cell dfnf401		
		
Cell drif101		
		
Cell invf101		
		
Cell invf104		
		
Cell labf111		

Original cell based on MOSIS 1.2 μm technology	Migrated cell based on TSMC 0.25 μm technology	Migrated cell based on TSMC 0.18 μm technology
		
Cell muxf201		
		
Cell muxf451		
		
Cell nanf201		
		
Cell norf201		
		
Cell orf301		

Original cell based on MOSIS 1.2 μ m technology	Migrated cell based on TSMC 0.25 μ m technology	Migrated cell based on TSMC 0.18 μ m technology
		
Cell sdnf401		
		
Cell swcf020		
		
Cell xorf201		

Original cell based on MOSIS 1.2 μ m technology	Migrated cell based on TSMC 0.25 μ m technology	Migrated cell based on TSMC 0.18 μ m technology
A four-bit buffer with high drive length		
A four-bit buffer with medium drive length		

Original cell based on MOSIS 1.2 μm technology	Migrated cell based on TSMC 0.25 μm technology	Migrated cell based on TSMC 0.18 μm technology
A four-bit programmable logarithmic shifter		
A four-bit two-input multiplexer		

Original cell based on MOSIS 1.2 μ m technology	Migrated cell based on TSMC 0.25 μ m technology	Migrated cell based on TSMC 0.18 μ m technology
A four-bit three-input multiplexer		
A four-bit bitwise NAND		

Original cell based on MOSIS 1.2 μ m technology	Migrated cell based on TSMC 0.25 μ m technology	Migrated cell based on TSMC 0.18 μ m technology
A four-bit bitwise NOR		
A four-bit pipeline true single-phase clocked register		

Original cell based on MOSIS 1.2 μm technology	Migrated cell based on TSMC 0.25 μm technology	Migrated cell based on TSMC 0.18 μm technology
A four-bit subtractor		
A four-bit tri-state buffer		

Bibliography

- [1] A.E.Dunlop. Slim-the translation of symbolic layouts into mask data. In *Proceeding of the 20st Design Automation Conference*, pages 595–602, 1980.
- [2] Michael A.Riepe and Karem A.Sakallah. The edge-based design rule model revisited. *ACM transactions on design automation of electronic system*, 3:463–486, July 1998.
- [3] Tom Burd. Very low power cell library. Technical report, University of California, Berkeley, 1995.
- [4] Chung-Kuan Cheng, Xiaotie Deng, Yuh-Zen Liao, and So-Zen Yao. Symbolic layout compaction under conditional design rules. *IEEE Transactions on Computer-Aided Design of Integrated Circuits and Systems*, 2:476–486, April 1992.
- [5] Y. E. Cho, A. J. Korenjak, and D. E. Stockton. FLOSS: An approach to automated layout for high-volume designs. In *Proceeding of the 14st Design Automation Conference*, pages 138 – 141, 1977.
- [6] Y.Eric Cho. A subjective review of compaction. In *22nd Design Automation Conference*, pages 396–404, 1985.
- [7] Dan Clein. *CMOS IC layout concepts, methodologies, and tools*. Newnes, 1999.
- [8] Ralph C.Mcgarity and Daniel P.Siewiorek. Experiments with the slim c i r c u i t compactor. In *Proceeding of the 20st Design Automation Conference*, pages 740–746, 1983.

- [9] David G.Boyer. Symbolic layout compaction review. In *25th ACM/IEEE Design Automation Conference*, pages 383–389, 1988.
- [10] Fook-Luen Heng, Zhan Chen, and Gustavo E.Tellez. A VLSI artwork legalization technique based on a new criterion of minimum layout perturbation. In *1997 International Symposium on Physical Design*, pages 116–121, 1997.
- [11] J.L.Burns and A.R.Newton. Efficient constraint generation for hierachical compaction. In *Proc. of the IEEE international conference on computer design*, pages 197–200, 1986.
- [12] Christopher Kingsley. A hiererachical, error-tolerant compactor. In *21st Design Automation Conference*, pages 126–132, 1984.
- [13] Chi-Yuan Lo and Ravi Varadarajan. An $o(n^{1.5} \log n)$ 1-d compaction algorithm. In *Proceeding of the 27th Design Automation Conference*, pages 382–387, 1990.
- [14] Juan Carlos Lopez, Roman Hermida, and Walter Geisselhardt. *Advanced techniques for embedded systems design and test*. Kluwer academic publishers, 1998.
- [15] David Marple. A hierarchy preserving hierarchical compactor. In *27th ACM/IEEE Design Automation Conference*, pages 375–381, 1990.
- [16] C. Mead and L. Conway. *Introduction to VLSI Systems*. Addison-Wesley, 1980.
- [17] M.Schiag, Y.Z.Liao, and C.K.Wong. An algorithm for optimal two-dimentional compaction of VLSI layouts. *Proceedings of ICCAD*, pages 88–89, 1983.
- [18] M.Y.Hsueh and D.O.Pederson. Computer-aided layout of lsi circuit building-blocks. Technical report, University of California, Berkeley, 1979.
- [19] John K. Ousterhout. Corner stitching: a data-structuring technique for vlsi layout tools. *IEEE transactions on computer-aided design*, 1:87–100, January 1984.

- [20] P.T.Chapman and Jr K.Clark. The scan line approach to design rules checking: computational experiences. In *Proceeding of the 21st Design Automation Conference*, pages 235–241, 1984.
- [21] Rochit Rajsuman. *System-on-a-chip: design and test*. Artech House, 2000.
- [22] Walter Scott and John Ousterhout. Magic maintainer’s manual #2: The technology file. Technical report, Lawrence Livermore National Laboratory and University of California, Berkeley.
- [23] Gerard Sierksma. *Linear and integer programming : theory and practice*. Marcel Dekker, 2002.
- [24] George S.Taylor and John K.Ousterhout. Magic’s incremental design rule checker. In *Proceeding of the 21st Design Automation Conference*, pages 160–165.
- [25] Neil Weste. Virtual grid symbolic layout. In *18th Design automation conference*, pages 225–233, 1981.
- [26] Wayne Wolf, Robert Mathews, John Newkirk, and Robert Dutton. Two-dimentional compaction strategies. *Proceedings of ICCAD*, pages 90–91, 1983.
- [27] Jianwen Zhu. Symbolic pointer analysis. In *Proceedings of the 2002 IEEE/ACM international conference on Computer-aided design*, pages 150– 157, 2002.